Universidade de Aveiro Departamento de Física
2015

João Gonçalo Ricardo Rodrigues

Variabilidade da pluma estuarina do Tejo: impacto na circulação e hidrologia costeira

The Tagus estuarine plume variability: impact in coastal circulation and hydrography

João Gonçalo Ricardo Rodrigues

Variabilidade da pluma estuarina do Tejo: impacto na circulação e hidrologia costeira
The Tagus estuarine plume variability: impact in coastal circulation and hydrography

Dissertação apresentada à Universidade de Aveiro para cumprimento dos requisitos necessários à obtenção do grau de Mestre em Meteorologia e Oceanografia Física, realizada sob a orientação científica do Doutor João Miguel Sequeira Silva Dias, professor do Departamento de Física da Universidade de Aveiro e co-orientação do Doutor Nuno Alexandre Firmino Vaz, investigador de pós-doutoramento da Universidade de Aveiro.

Este trabalho foi desenvolvido no âmbito do projeto BioChangeR (PTDC/AAC-AMB/121191/2010)

o júri / the jury

presidente / president

Prof. Doutor José Manuel Henriques Castanheira
Professor auxiliar do Departamento de Física na Universidade de Aveiro

vogais / examiners committee

Doutor Paulo Miguel Chambel Filipe Lopes Teles Leitão
Consultor, HIDROMOD, Modelação em Engenharia, Lda.

Prof. Doutor João Miguel Sequeira Silva Dias
Professor auxiliar com agregação do Departamento de Física na Universidade de Aveiro

acknowledgements

This study was only possible by the encouragement and collaboration of diverse people.

First of all, thanks to Prof. Doctor João Miguel Dias, for his scientific supervision and helpfully assistance.

To my supervisor, Doctor Nuno Vaz, a special thank for his scientific supervision, idea sharing and assistance in the development of this study.

Thanks to all colleagues from Núcleo de Modelação Estuarina e Costeira (NMEC), specially to Renato Mendes, for increasing the entropy of my thoughts and giving useful ideas for the study development.

Thanks to HIDROMOD group for the friendly environment and help in the MOHID compilation process.

Thanks to MARETEC group, specially to Francisco Campuzano for the PCOMS data providing.

Thanks to my parents, João and Regina for believing that I will finish my MSc one day, and to my sister, Sara for letting me finish the MSc thesis before her.

To the little ones, Matilde, Sofia and Leonor.

Thank you Soraia for all your help in the moments I most needed.

palavras-chave

Estuário do Tejo, modelo hidrodinâmico, pluma estuarina, MOHID, SOM, MODIS

resumo

As descargas dos estuários formam uma pluma que é advetada para a região costeira adjacente, durante a maré vazante, modulando a circulação e hidrografia costeiras. Na costa central portuguesa, a pluma do Estuário do Tejo influencia a hidrografia da região, controlando a dinâmica local. Na atualidade, estudos de plumas estuarinas são realizados utilizando modelos de circulação e de transporte de alta-resolução e sofisticados métodos de análise de dados, como as redes neuronais. O objetivo deste estudo consiste em analisar os padrões da descarga estuarina do Tejo na zona costeira adjacente, sob diferentes condições de vento e eventos de descarga estuarinas elevadas.

Neste âmbito, implementou-se o modelo 3D de circulação e transporte MOHID, utilizando um método de downscaling do modelo Operational Model for the Portuguese Coast (PCOMS) (6 km) para a ROFI do Estuário do Tejo (500m). De modo a melhorar os forçamentos atmosféricos do modelo costeiro, implementou-se uma nova aplicação de alta-resolução (2 km) do modelo WRF para a região. A validação dos modelos de circulação e de transporte foram realizadas para o período de Julho a Dezembro de 2012. Resultados numéricos demonstram uma reprodução correta dos padrões superficiais quando comparados com dados observados de velocidade da corrente, salinidade e temperatura da água. O erro médio quadrático (RMSE) das correntes de superfície mostrou um desvio médio inferior a 16 cms^{-1}. Comparação da temperatura superficial da agua com os dados remotos do sensor MODIS-Aqua identificaram um desvio inferior a 2°C, demostrando a qualidade das previsões do modelo em reproduzir os padrões dinâmicos costeiros.

De modo a estudar a variabilidade costeira causada pela descarga estuarina do Tejo, simularam-se 5 cenários utilizando ventos favoráveis de upwelling e downwelling, e descargas do Rio Tejo de 1500, 3000 e 5000 m^{3}s^{-1}. As simulações dos cenários foram realizadas para o período de 8-31 de Novembro de 2012, devido à ocorrência de padrões favoráveis de vento. Com o objetivo de quantificar a variabilidade costeira, realizou-se uma analise SOM com 1x4 padrões espaciais dos campos de salinidade à superfície. Os resultados demonstram que as descargas fluviais são o principal forçamento nas simulações, só superados pelo vento aquando se registam baixas descarga fluviais. Secções transversais da salinidade mostraram uma profundidade da pluma estuarina com cerca de 15 m na zona da embocadura do estuário, reduzindo-se para 10 m na zona costeira adjacente ao Cabo da Roca. A tensão do vento revelou ter um papel importante na dispersão da pluma, sendo responsável pelo transporte para norte ou para sudoeste da mesma. Em todos os cenários, os ventos favoráveis a downwelling transportam a pluma para norte encostada à costa, enquanto ventos de upwelling transportam a pluma para sudoeste.

A nova implementação de alta resolução em 3D desenvolvida neste trabalho permite retirar informação extra acerca da dinâmica da pluma estuarina sob diferentes condições de vento e descarga do Rio Tejo. Padrões distintos de dispersão foram observados, permitindo uma melhoria do conhecimento da circulação e hidrografia da região. Para trabalhos futuros, este modelo pode permitir o acoplamento de modelos biogeoquímicos ou de derrame de hidrocarbonetos, temas importantes e desafiantes para a complexa zona costeira adjacente ao Estuário do Tejo.

keywords

Tagus estuary, hydrodynamic model, estuarine plume, MOHID, SOM, MODIS

abstract

Buoyant discharges from estuaries form an outflow plume that is advected onto the near shelf during the ebb tide, modulating the circulation and hydrography of the adjacent coast. In the central coast of Portugal, the plume from the Tagus Estuary influences the hydrography of the area, controlling local dynamics. Nowadays, estuarine plume propagation studies are performed using high-resolution circulation and transport models and sophisticated data analyses tools, as the artificial neural networks. The main aim of this work consists in studying the Tagus Estuarine outflow behaviour under different wind forcing conditions and variable river discharge events.

For this purpose, a 3D circulation and transport model (www.mohid.com) was implemented for the region, using a nested downscaling approach from the Operational Model for the Portuguese Coast (PCOMS) (6 km) to the Tagus ROFI (500 m). To improve the atmospheric circulation model forcing, a new high-resolution atmospheric model (2 km) was implemented for the region, using the WRF model. To validate the circulation and transport models, a simulation period between July and December 2012 was used. Numerical predictions shown an accurate reproduction of the surface patterns when compared with observed data of current velocity, salinity and water temperature. The root mean square error (RMSE) of surface currents revealed a mean deviation lower than 16 cm s^{-1}. SST comparison with MODIS-Aqua remote sensing imagery shows a deviation lower than 2°C, revealing the model accuracy in reproducing coastal dynamics.

In order to study coastal variability due to the Tagus estuarine outflow, five scenarios were simulated under upwelling and downwelling favourable winds and Tagus river discharge of 1500, 3000 and 5000 m^3s^{-1}. The scenarios simulations were performed for the days 8-31 of November 2012 because of favourable distinct wind patterns. In order to quantify the region variability 1×4 Self-Organizing Map (SOM) of the surface salinity fields were performed. The results show that river discharge is the main controlling forcing for the scenarios simulation, only overtaken by the wind, when low discharge values were present. The cross-shelf sections show a depth of the plume bulge of 15 m near the mouth of the estuary, reducing to 10 m in the far region, near *Cabo da Roca*. The wind stress played a powerful role in the dispersion of the bulge, being responsible for the north or southwest transport of the plume. In all scenarios, under downwelling favourable winds the plume is compressed toward the coast, and under upwelling winds the plume follows a SW direction, being advected offshore.

The new high resolution 3D implementation developed in this study provides extra information about the Tejo estuarine plume dynamic under different conditions of winds and river discharge. Distinct spatial dispersion was observed improving the knowledge of the region circulation and hydrography. Thus, this validated implementation can be used for new studies, such as coupling of a biogeochemistry or oil spill models, topics that are important and challenging for a complex coastal region such as the off the Tagus Estuary.

Contents

List of Figures

List of Tables

List of Acronyms

ADCP Acoustic Doppler Current Profiler

ANN Artificial Neural Network

APA *Agência Portuguesa do Ambiente*

BMU Best-Matching Unit

Discharge1 1500 m^3s^{-1}

Discharge2 3000 m^3s^{-1}

Discharge3 5000 m^3s^{-1}

EMG *Estação Meteorológica da Guia*

ENACWst Eastern North Atlantic Central Water sub tropical branch

EOF Empirical Orthogonal Functions

FES2004 Finite Element Solution 2004

FN Form Number

FORTRAN IBM Mathematical Formula Translation System

GDOP Geometric Dilution of Precision

GFS Global Forecast System

HF High-Frequency

IH *Instituto Hidrográfico*

IST Instituto Superior Técnico

MARETEC Marine and Environmental Technology Research Center

MODIS Moderate Resolution Imaging Spectroradiometer

MOHID Water Modelling System

nLw normalized waterleaving radiances

N North

NE Northeast

NNE North-northeast

NNW North-northwest

NW Northwest

PC Portuguese Current

PCC Portugal Coastal Current

PCCC Portugal Coastal Counter Current

PCOMS Portuguese Coast Operational Modelling System

RMSE root mean squared error

ROFI region of freshwater influence

ScA Scenario A

ScB Scenario B

ScC Scenario C

ScD Scenario D

ScE Scenario E

SOM Self-Organizing Map

SIMOC *Sistema de Monitorização Operacional de Correntes Costeiras*

SSE sea surface elevation

SST sea surface temperature

SSS sea surface salinity

WRF Weather Research and Forecasting model

UNESCO United Nations Educational, Scientific and Cultural Organization

Chapter 1

Introduction

1.1 Motivation and aims

Coastal hydrography is highly affected by the interaction between land, water and atmospheric forcing. Both forcings are very much influenced by natural and anthropogenic factors, being crucial to analyse the joint influences.

In general, in studies of coastal processes, estuarine regions are not included, since estuaries and near coastal regions are preferentially treated separately because of spatial resolution needed to represent local physical processes (Otero *et al.*, 2008; Oliveira *et al.*, 2009). Estuaries are usually related with zones of high primary productivity, nurseries for fish species, sheltering for vessels and harbour industries. These characteristics contributes to a population increase around estuaries borders that can increase the anthropogenic stress.

Usually, the impact of estuaries in the coastal region is in the form of a buoyant plume, that affects circulation and transport of soluble and particulate materials to the near coast. These plumes are dynamical structures resulting from the discharge of low salinity water over a heavier (denser) ambient (Kourafalou *et al.*, 1996). The plumes can change physical, chemical and biological features of those regions and also effect the transport of soluble and suspended materials that can lead to an increase in coastal primary production (Sousa *et al.*, 2013).

The pressure caused by anthropogenic factor in estuaries and coastal systems may turn these regions into vulnerable systems, requesting frequent monitorization and damage control.

The central region of Portugal, comprising the Tagus Estuarine region, is influenced by

numerous storms which can impact coastal systems due to strong winds and considerable amount of precipitation, promoting changes in circulation and hydrography.

Another forcing that affects estuarine and coastal dynamics is the freshwater discharge, which is quiet important once the Tagus river drains one of the largest watershed areas of the Iberian Peninsula, retaining a huge amount of precipitable water able to produce high river discharge. That can have a major impact in the estuary (Vaz and Dias, 2014). Moreover, according to Dagg *et al.* (2004) river outflows can be related with the plume extension in the near coastal region.

Another forcing that influences estuarine and coastal circulation is the wind intensity and direction. In fact, the typical wind pattern in the Portuguese west coast, during the summer, is from the north. These winds are commonly referred as upwelling favourable, since they promote an offshore advection of surface waters and a vertical advection of rich nutrient upwelled waters toward the surface. During these upwelling events an increase in primary productivity can be observed (Vaz *et al.*, 2015).

Several studies have been performed regarding the Tagus estuary dynamics. Nevertheless there are not many studies regarding the adjacent coastal region circulation. Only a few studies have been performed for the near coastal region of the Tagus Estuary. In fact, Fortunato *et al.* (1999) and Vaz *et al.* (2009b, 2011, 2015) studied the region close to the estuary mouth, highlighting topics as the mouth hydrodynamics, coastal circulation and surface sea surface temperature (SST) and chlorophyll patterns.

The main objective of this study is to highlight the main features of the Tagus estuarine plume under different wind stress and freshwater discharge conditions in order to increase the knowledge of the impact of the large estuarine discharge in the hydrography and circulation of the region. To achieve these goals, a nested implementation of an high resolution circulation model (based on MOHID) is used. Also, a recent methodology to compute the main variability is also used, the self-organizing maps (SOM) method. Merged with the main objective, there are important steps for model validation using different datasets, such as: sea surface elevation (SSE) from tide gauge, surface current validation using *Sistema de Monitorização Operacional de Correntes Costeiras* (SIMOC) and Moderate Resolution Imaging Spectroradiometer (MODIS) data.

1.2 Literature review

1.2.1 Estuarine plumes

Estuarine plumes impact in the coastal ocean in the form of a buoyant plume that transports land and rainfall materials from the river discharge. From the dynamical point of view, the discharge area of rivers in the coast can be considered as an input of momentum and buoyancy caused by the release of a less dense fluid (river discharge) into a heavier fluid (coastal waters). This structure is known as buoyant river plume (Kourafalou *et al.*, 1996).

Thus structures are vital for the transport of sediments, nutrients and organic mater from estuaries to the near coast, playing an important role in their transport.

The main characteristics of these plumes have been studied since the early 50's of the XX century using numerical model applications. One of the first studies were realized by Takano (1954a,b, 1955) using an idealized model with a straight coast. In the following years the impact of diverse river plumes was analyzed using numerical model applications: as examples are the Columbia River Estuary (USA) (Stefnsson and Richards, 1963), Chesapeake Bay (USA) (Boicourt, 1973) and the Connecticut River Estuary (USA) (Garvine, 1974).

The characterization of the plume anatomy was studied, firstly, by Garvine (1982). The author split the surface plume in three regions: source, near-field and far-field plume. These regions have distinct characteristics and also different impact in the transport of soluble and dissolved materials. More recently, Horner-Devine *et al.* (2009) have proposed an alteration to the previous classification, decomposing the near-field plume in pulse, tidal plume and residual re-circulating plume.

Also, the influence of submarine canyons in plume outflow was studied by Weaver and Hsieh (1987). Here the authors observed that in the presence of a canyon near the estuary mouth, the joint effect of baroclinicity and relief provides a strong forcing term for the barotropic flow, resulting in an along shelf propagation of the plume where is observed an increase of the energy; following the previous study, Chao (1988) has concluded that the existence of a shelf slope reduces the seaward excursion of the plume bulge.

The influence of the estuarine outflow in the adjacent coastal shelf was also identified by Yankovsky (2000). In this work, the role of the outflow channel shape and the width-to-depth ratio of the estuary mouth was observed, revealing an important role in dynamics of the plume.

Kourafalou *et al.* (1996) identified the plumes structure for different wind stress scenarios, and they have found that during favourable downwelling wind, the plume enhanced the effect

of the coastal current in the region, confining the buoyancy close to the coast. Conversely, favourable upwelling winds produce a larger offshore plume propagation (or expansion). The same conclusion was obtained by Hickey *et al.* (1998), Fong and Geyer (2001) and Fong and Geyer (2002) in their studies.

During the last decade, the plume dynamics of several Portuguese estuaries has been studied. In 2010, Mendes had implemented a circulation and transport model for the Ria de Aveiro Lagoon, classifying it as near-field and surface-advected plume, according to the Hetland (2005) proposed methodology. Sousa *et al.* (2014a,b) evaluated the influence of the Minho river in the Rias Baixas (NW Spain) hydrography using different wind pattern and river discharge scenarios. Those authors concluded that under northward wind, the Minho river plume can reach *Ria de Pontevedra* (Spain).

For the adjacent area of the Tagus estuary there are a few studies about plumes propagation and characteristics. One of the first analysis of the plume propagation behaviour was realized by Vaz *et al.* (2009b). These authors studied the estuarine plume propagation based on a nested 3D baroclinic model with 35 vertical layers highlighting the impact of the Tagus Estuarine plume in the coast. Offshore Ekman transport induced by southward winds produces a maximum displacement of the plume water of about 40 km offshore. Also, Valente and da Silva (2009) have studied the turbid signal in the Tagus Estuary mouth using a 3 year sequence of MODIS-Aqua nLw551 satellite product, concluding that the plume has a fortnightly scale variation, presenting small dimensions after neap tides and higher dimensions after spring tides. The dimension of the turbid area can increase with river discharge and winds which are consistent with the results obtained by Mendes *et al.* (2014) for the Douro river plume, where was not observed an evidence of an existing plume for river flow lower than 148 m^3s^{-1}.

More recently, Vaz *et al.* (2015) reveal the impact of Tagus estuary plume in adjacent coastal waters properties, such as, water temperature, salinity and chlorophyll concentration. In their study, the authors propose as future work, the implementation of better atmospheric forcing, justified by the existence of topographic features, such as *Serra de Sintra*, which can influence the impact of the Tagus estuarine plume in the circulation and hydrography of the adjacent coast.

1.2.2 Circulation model - MOHID

The use of circulation models brings a strong forecasting and hindcasting capability to the study of coastal and estuarine areas. One of those models is the numerical model Water Modelling System (MOHID), a 3D baroclinic finite volume marine model designed for the study of estuarine and coastal regions. This model uses several modules to compute circulation, water properties transport and biogeochemical features of estuarine and coastal systems, being possible the addition of new ones, once that the model is an open source code.

MOHID is used in many different systems, presenting a large versatility. As examples, Gomez-Gesteira *et al.* (1999) evaluated the residence time of the NW region of Spain, taking advantage of the particle tracking module. Saraiva *et al.* (2007) have used MOHID to investigate the impact of nutrients loads in the main Portuguese estuaries, while Sousa *et al.* (2013) evaluated the Minho river plume dynamic and its influence in the Rias Baixas.

The Ria de Aveiro lagoon has been also studied during the last years thought the application of MOHID. In fact, studies focused on circulation (Vaz *et al.*, 2007; Picado *et al.*, 2013) and transport of properties (Vaz *et al.*, 2009a; Mendes, 2010) were performed in order to fully characteriz the lagoon's hydrodynamics. The impact of bathymetric changes in the Lima estuary hydrodynamic were investigate by Rodrigues *et al.* (2012) using also MOHID.

Moreover, the hydrodynamic of the Tagus Estuary has been studied through numerical experiments based on MOHID applications. Leitão *et al.* (2000) implemented a 3D application for the Tagus region of fresh water influence in which, the authors observed the influence of *Serra de Sintra* in the rotation of the wind field capable of generate strong barotropic currents. Fernandes (2005) implemented an operational application for the Tagus Estuary and Vaz *et al.* (2009b) take one first step on the characterization of the Tagus estuarine plume. In the following years several circulation and water transport studies were performed in order to highlight the estuarine and coastal features of the system, evaluating aspects as the tidal propagation, residual circulation and cohesive sediments dynamics (Vaz *et al.*, 2011; Dias *et al.*, 2013; Vaz and Dias, 2014; Franz *et al.*, 2014). One recent work studies the SST and chlorophyll in the adjacent region of the estuary (Vaz *et al.*, 2015).

This model was also used to study the hydrodynamics and transport process at other estuarine system. In fact, Coelho *et al.* (2000) conducted a circulation and water transport study in Guadiana Estuary, where they concluded that with river discharger higher then 1000 $m^3\ s^{-1}$ fulfil the entire estuary with fresh water. A Sado Estuary implementation of

MOHID was performed by Martins *et al.* (2001) using a generic vertical discretization to highlight estuarine dynamics in the system. A 3D implementations for the Lagoon of Ria Formosa was performed by Silva *et al.* (2002) aiming to understand the Faro-Olhão inlet processes. The effect of coastal waves on sea level inside Obídos Lagoon was assessed by Malhadas *et al.* (2009), where results showed that lagoon sea level remains above offshore sea level during storm wave periods.

The versatility of MOHID system allows the necessary conditions to be used as a operational model. In fact, the Technical University of Lisbon (UTL) used the Portuguese Coast Operational Modelling System (PCOMS) based on MOHID application, that covers all the continental Portuguese territory to produce daily forecast of coastal circulation, hydrography and biogeochemistry (oxygen, chlorophyll and nutrients) maps (Mateus *et al.*, 2012).

1.2.3 Self-Organizing Maps (SOM)

Coupled ocean-atmosphere datasets from observations and numerical model output are steadily increasing the amount of available data to produce estuarine and coastal studies (Liu and Weisberg, 2005). Petrou (2004) estimates that less of 5% of all remote sensing images are ever seen or used by the scientific community. Therefore, new pattern detection techniques have been developed to analyse those datasets.

The non-linearity of ocean and atmospherics dynamic make the pattern recognition harder and challenging. One of those new techniques is the Self-Organizing Map (SOM), an unsupervised neural network based on competitive learning (Kohonen, 1988; Vesanto *et al.*, 2000). To demonstrate the SOM capability, Liu *et al.* (2006b) have performed a comparative test using the sum of a sinusoidal wave and concluded that SOM successfully identified all the input wave periods. Futher studies by Liu and Weisberg (2007) concluded that the SOM patterns were more intuitive and accurate than the principal mode of the Empirical Orthogonal Functions (EOF) method.

SOM algorithm implementation in climatology field began in the late 1990s, using daily sea level pressure data to identify atmospheric circulation patterns (Hewitson and Crane, 2002), sea level patterns over North Atlantic Region (Schuenemann and Cassano, 2010) and air temperature and humidity spatial variability (Reusch *et al.*, 2005). Also, Kropp and Klenke (1997) have used SOM for the analysis of 170 sediments samples with different biological and geochemical conditions, concluding that SOM managed to shrink a 11-dimensional data manifold into a 2-dimensional subspace preserving all relevant features

of the data set.

Richardson *et al.* (2003) and Risien (2004) retrieve surface pattern currents and variability of the Benguela upwelling region (Southeaster Atlantic), while Cheng and Wilson (2006) used SOM to identify vertical pattern of currents for the Hudson River estuary (USA) using 233 day Acoustic Doppler Current Profiler (ADCP) segments.

Liu and Weisberg (2005) and Liu *et al.* (2006a,b, 2007) have characterized the West Florida Shelf region (USA) using different datasets (SST, High-Frequency (HF) radar and ADCP). Liu *et al.* (2009) used a 3D model dataset, for the region of Columbia River (USA), to identify the pattern of estuarine plume, highlighting its bi-directional propagation. The authors observed the influence of wind on the plume dimension, with a smaller bulge under downwelling wind events and larger bulges under upwelling wind events.

1.3 Structure of this work

Concerning the structure of this dissertation it was divided in five chapters. Chapter 1 presents a description of the main objectives and a literature review of relevant aspects to the study. In Chapter 2, a detailed description of the study region, giving special focus to the adjacent coastal area of Tagus estuary, is performed. In Chapter 3, the numerical model implementation and methodology followed during thesis are described.

The results and discussion of the validation and scenarios results are presented in Chapter 4. Finally, in Chapter 5 an overview of the results, presenting final conclusions and providing some future research suggestions is made.

Chapter 2

Study Region

The study region is located on the Portuguese central west coast between 38.0°N and 39.5°N, and comprises the Tagus Estuary and the near coastal ocean (Figure 2.1). This region is located in a highly populated region, subject to an enormous natural and human stress. The topography of the adjacent region of Tagus estuary is considered relatively flat, with the 200 m isobath located roughly at 30 km offshore of Tagus estuary mouth. However the area comprises a complex bathymetry, constituted by three submarine canyons: the

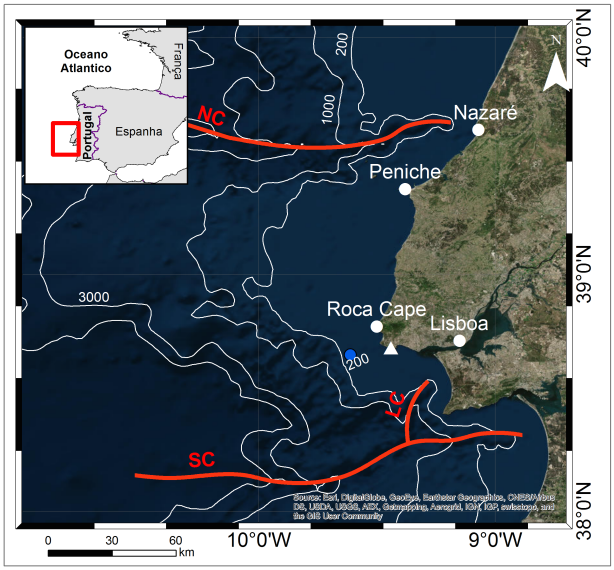

Figure 2.1: The study area comprising the Tagus Estuary and the adjacent shelf region. White lines represent isobaths of 200, 1000, 3000 and 4000 m. Red lines depicts the Setubal (SC), Lisbon (LC) and Nazaré canyons (NC) locations. Blue circle represent QuickScat location and white triangle the EMG.

Nazaré, the Lisbon and the Setubal canyons. These canyons extend beyond the 10°N with more than 2000 m depth.

The wind regime in the region is strongly influenced by the Azores high-pressure system. The pressure difference between the centre of Azores high-pressure and Portugal varies from 1 mbar in winter to 8 mbar in the Summer. This gradient is responsible by the rise of strong north/north-westerly winds, affecting the region (Fiúza *et al.*, 1982).

In this region, wind-driven upwelling occurs when equatorward winds induce net offshore Ekman surface transport, resulting in a divergence of nearshore transport, conversely favourable downwelling winds induce an Ekman surface transport toward the coastal region (Fiúza *et al.*, 1982; Silva, 2008).

In adition to the wind effect on coastal currents, the Portuguese west coast presents an generally equatorward flow, known as the Portuguese Current (PC). PC is characterized as an upper circulation flow with little seasonality that extends from the 10°W to about 24°W (Maillard, 1986). In the continental shelf, during autumn and early winter, a north poleward flow (near the 200 m depth) is observed. This is known as the Portugal Coastal Counter Current (PCCC) (Ambar and Fiúza, 1994). This flow results from the geostrophic adjustment of weak eastward oceanic flow, driven by the large-scale meridional baroclinic pressure gradient (Frouin *et al.*, 1990; Pérez *et al.*, 2001). During the upwelling season, PCCC fades because of the northerly winds, giving place to the Portugal Coastal Current (PCC). Both currents are typically located in a narrow band between $10 - 11$°W (Pérez *et al.*, 2001). All these coastal currents may act to change the propagation pattern of the Tagus estuarine plume, since they can intensify (or de-intensify) the wind and estuarine discharge currents.

According to Mason *et al.* (2005), the main water source of the upper layers (>300 m) of the West Iberian coastal waters is the Eastern North Atlantic Central Water sub tropical branch (ENACWst). During upwelling events, ENACWst is the main source of the advected water south of Nazaré canyon and, according to Ríos *et al.* (1992) the main observed water source in the Lisbon bay.

2.1 Tagus Estuary

Estuarine circulation and exchange processes are forced by tide, freshwater discharges and atmospheric conditions. It is fundamental to assess the circulation and hydrographic characteristics of the estuary, once that these will have a direct role on the estuarine-coastal

exchange.

The Tagus Estuary covers an area of about 320 km^2 of which 40% are tidal flats (Silva, 2012). It is the largest estuary of the Iberian Peninsula and one of the most extensive wetlands in Portugal (Dias, 1993). On its shores is located the highest population density zone of Portugal, the metropolitan region of Lisbon (Figure 2.2).

The estuary has a pear-shape with roughly 30 km long and can be morphologically split in three distinct zones (Rusu *et al.*, 2009; Neves, 2010):

- An upstream area with low average depth ($\sim$ 2 m), presenting large intertidal zones. Here, the connection with the river is made through a channel with an average width of 200 m (location in 38.86ºN, 9.03ºW);

- The Central area (known as *Mar da Palha*) with an average depth of 7 m. This zone is the largest of the estuary, reaching 15 km wide. In this zone freshwater is mixed with the ocean water (located between 38.65ºN, 9.12ºW and 38.86ºN, 9.03ºW);

- The inlet channel or corridor (known as *corredor*) has 15 km length and is 2 km wide and present the deepest area of the estuary, with a maximum depth of about 40 m. This region is the connection with the ocean and presents the faster flow, over 2 ms^{-1} (Vaz *et al.*, 2011) . The mouth of the estuary is usually considered the section São Julião da Barra - Bugio.

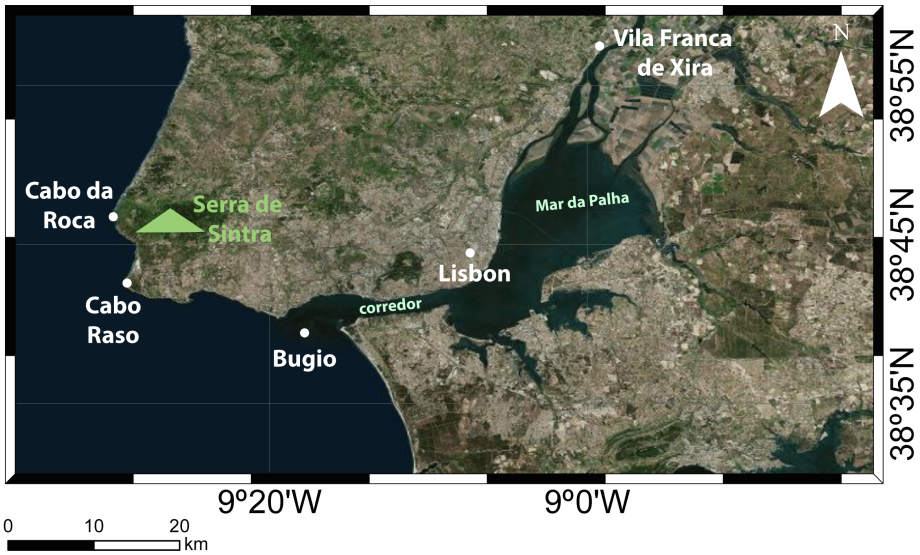

Figure 2.2: Tagus Estuary region.

The estuary hydrography is mainly controlled by the tidal propagation and fluvial discharge (Vaz *et al.*, 2011). The estuary is mesotidal, with a typical neap tide of 0.8 m and spring tide of 4.0 m (Fortunato *et al.*, 1997). The tide has a dominant role in the estuary dynamics, since the tidal prism is on the order of 600×10^6 m^3 in comparison with the 8.2×10^6 m^3 of river flow *per* tidal cycle (Neves, 2010).

According to Fortunato *et al.* (1999), floods take normally one hour more in comparison to ebb, leading to a dominant ebb flow. This ebb dominance results in higher current velocities during ebb, reaching 2 ms^{-1} in spring tides (Portela, 1996; Vaz and Dias, 2014).

2.1.1 River discharge

The main freshwater tributary of the estuary is the Tagus river. The river rises in Serra de Albarracin (Spain) and travels around 1000 km before discharging in the Atlantic Ocean near Lisbon. In its route, drains a basin which is the second largest of Iberian Peninsula reaching almost 81 000 km^2, of which 30% are in Portuguese territory (Vis *et al.*, 2010).

The Tagus river discharge usually presents pronounced annual and inter-annual variations (Vale and Sundby, 1987). The discharge regime becomes modulated after the 50's decade of the XX century after the building of several dams in the Tagus river basin (Macedo, 2006). The annual average discharge of Tagus river is between 300-400 m^{3}s^{-1} (Macedo, 2006; Neves, 2010; Vaz *et al.*, 2011) but monthly averages can vary between 1 m^{3}s^{-1} and 2200 m^{3}s^{-1} (Loureiro, 1979). The estuarine freshwater budget is controlled by the inflow of three main rivers (Tagus, Sorraia and Trancão rivers). A statistical analysis for these rivers inflow was performed using daily river discharge data available from *Agência Portuguesa do Ambiente* (APA) website (snirh.pt). The Tagus river analysis was performed using data from the the Ómnias station (18E/04H) for a period ranging between 1978 and 2001. For this period an average discharge of 335 m^{3}s^{-1} was observed.

The other two rivers (Sorraia and Trancão) display a lower average annual discharge, when compared to the Tagus River (Figure 2.3a). As for both rivers there are no monitoring stations available near the connection with the Tagus estuary, were considered the nearest measuring stations to the discharge point. For the Sorraia River, data from the stations of the *Ponte de Coruche* (20F/02H) and *Ponte de São Estevão* (20E/02H) were used, for the period of 1976-1980. The same approach was implemented for the Trancão River, using the stations of *Ponte Canas* (20C/01H) and *Ponte Pinhal* (21C/01H), for a period between the years of 1979 and 1989. From the data analysis annual river discharges of 39.3 m^{3}s^{-1} and 1.7 m^{3}s^{-1} for Sorraia and Trancão rivers, respectively. These values are consistent with

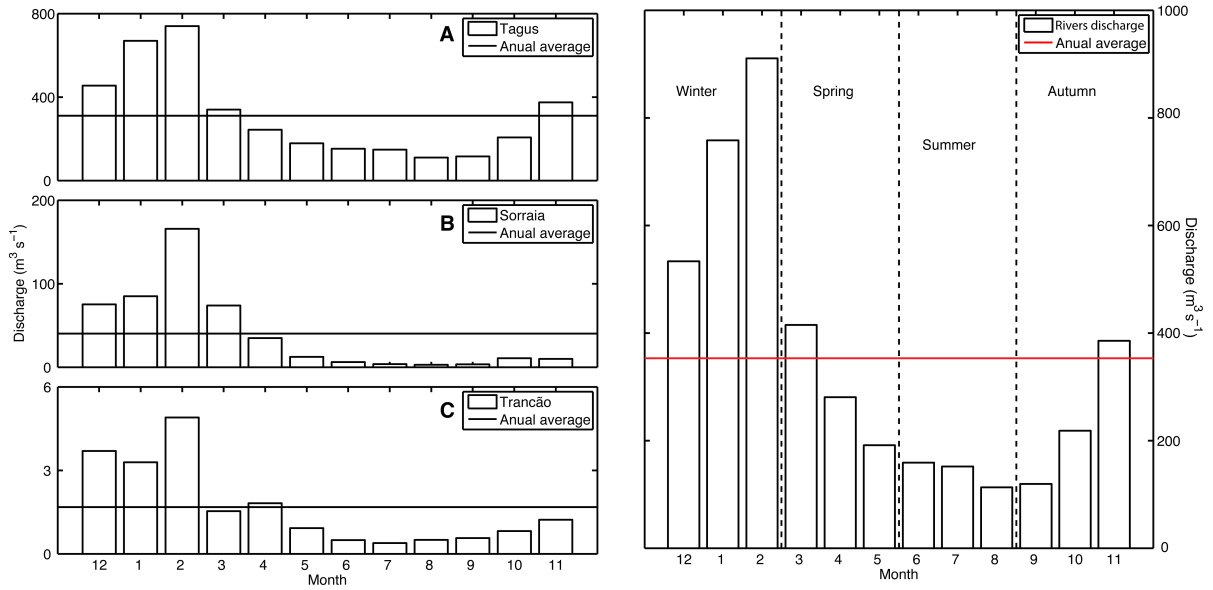

(a) (b)

Figure 2.3: (a) monthly mean rivers discharge values of (A) Tagus, (B) Sorraia and (C) Trancão rivers, calculated from daily discharge values. (b) the sum of rivers discharges to the estuary.

those found by Fortunato *et al.* (1999) (with 35 and 2.5 m^3s^{-1}, respectively).

From Figure 2.3b a strong seasonality on total freshwater discharge to the estuary is observable, with higher values registered during the winter period. On the other hand, during the summer the freshwater discharge is considerable low. The statistical analysis of freshwater discharge in the estuary reveals that the Tagus River contributes with 80% of the total inflow, leaving 19% to the Sorraia River and less than 1% to the Trancão River.

In Tagus River, during winter, 5% of the discharge observations are lower than 44 m^3s^{-1} or higher then 1875 m^3s^{-1}, showing high variability (Table 2.1). In Summer, the variability is lower, with 5% of observations below 14 m^3s^{-1} or over 340 m^3s^{-1}.

Table 2.1: Daily Tagus river discharge percentiles for the period 1978-2001.

Percentiles	**Winter** m^3s^{-1}	**Spring** m^3s^{-1}	**Summer** m^3s^{-1}	**Autumn** m^3s^{-1}
5	44	28	14	17
50	302	156	102	150
95	1875	930	340	801

2.2 Wind influence

The influence of the wind stress on ocean surface circulation and hydrography has been largely observed on plumes and other oceanographic features (Sousa, 2013). For the study region, upwelling regimes are highly dependent of the northern wind stress component (Vaz *et al.*, 2009b). Therefore, the use of inaccurate surface wind intensity and direction, as atmospheric forcing may modify the circulation model results. Thus, an accurate reproduction of wind patterns is a key point for numerical model applications, especially for a study region characterized by its large spatial variability. To illustrate this, three wind roses generated with data for the full years of 2004-2008 at three locations (Figure 2.4), located 50 km apart of each other, are presented in Figure 2.5.

The QuickScat data corresponds to daily remote sensing wind sensor observations. These data show a predominance of winds from N and NNW, with 19.6% and 16.7% of occurrence, respectively (Figure 2.5a). Regarding the *Estação Meteorológica da Guia* (EMG) station, representative of the Tagus estuary mouth, a N (17.0%) and NNE (16.4%) wind predominance for the same period was observed (Figure 2.5b). Finally, the station near the Lisbon airport shows a NW/NNW predominance with 18.5% and 18.2%, respectively (Figure 2.5c).

These results suggest a strong spatial wind variability in the study region, both in terms of wind intensity and direction. The presence of the *Serra de Sintra*, 20 km north of EMG, that might be the reason for the rotation of dominant winds and intensity changes. These

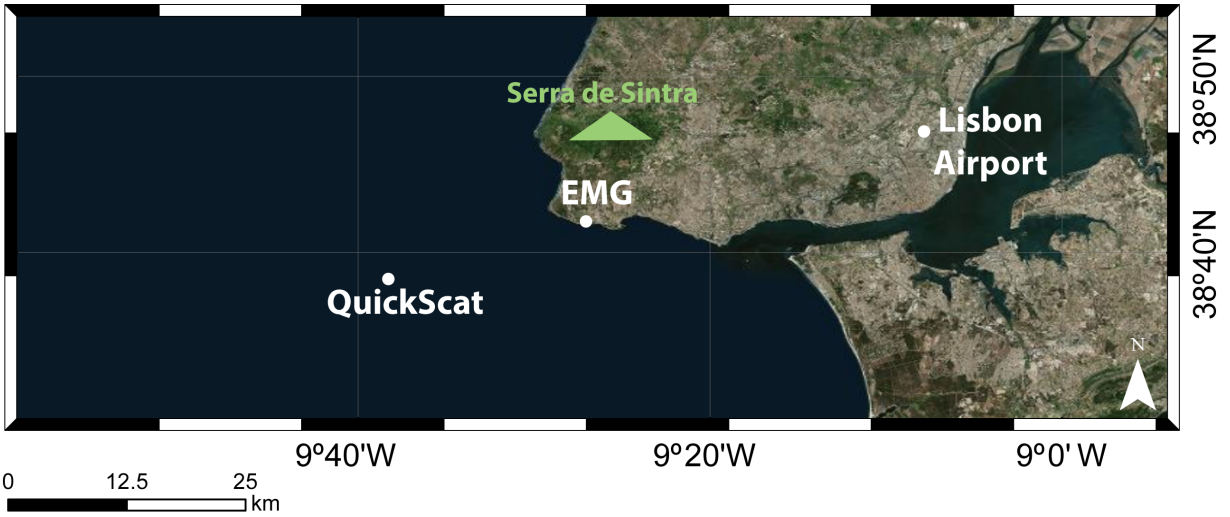

Figure 2.4: Location of the wind comparison points.

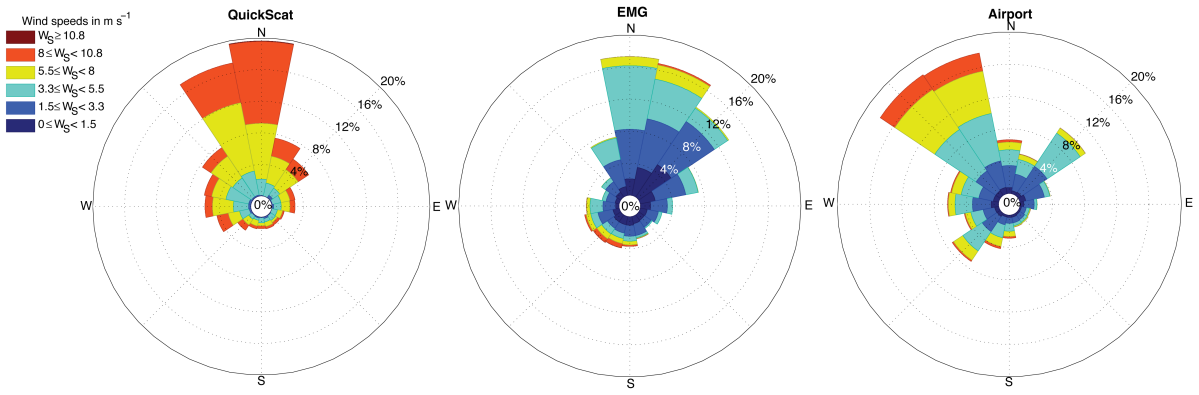

(a) QuickScat sensor. (b) EMG station. (c) Airport Station.

Figure 2.5: Statistical analysis of wind intensity and direction for: (a) QuickScat sensor, (b) EMG station and (c) airport station.

results show the importance of the application of a high-resolution atmospheric model to provide accurate boundary conditions to the coastal/oceanic circulation model.

Chapter 3

Numerical Models and Methodology

3.1 Circulation model

In this study an implementation of MOHID (*MOdelação HIDrodinâmica*) is used. MOHID is a three-dimensional model developed and maintained by the Marine and Environmental Technology Research Center (MARETEC) at Instituto Superior Técnico (IST). This open-source project allows any person to submit a new set of functions to the model. Open-source models permit researchers from different areas to give further contributes to the models.

The first version of MOHID stacks back to the middle 80's of the XX century, when the model was only a two-dimensional tidal model written in IBM Mathematical Formula Translation System (FORTRAN) 77 (Neves, 1985). Since then, MOHID has suffered significant advances, such as: three-dimensional capacity (Santos, 1995), lagrangian transport module (Leitão, 1996) and water quality modules (Miranda, 1997).

One important feature of MOHID is the ability to simulate estuarine environments (Vaz *et al.*, 2007; Malhadas *et al.*, 2009; Franz *et al.*, 2014; Vaz and Dias, 2014; Vaz *et al.*, 2015), and also, large scale circulation (Leitão *et al.*, 2005; Vaz *et al.*, 2009b; Sousa *et al.*, 2014a,b). To accomplish the objectives of this work two model applications were implemented: one for the estuarine area and other for the coastal adjacent area.

3.1.1 Physical descritization

MOHID solves the three-dimensional incompressible primitive equations assuming hydrostatic equilibrium and the Boussinesq and Reynolds approximations. The primitive

equations are solved in Cartesian coordinates for incompressible flows. The following equations have been derived taking into account these approximations and more details can be obtained in Santos (1995), Leitão (2003) and Vaz (2007).

The momentum and mass balance equation are:

$$\frac{\partial u_i}{\partial t} + \frac{\partial \left(u_i u_j\right)}{\partial x_j} = -\frac{1}{\rho 0}\frac{\partial p_{atm}}{\partial x_1} - g\frac{\rho(\eta)}{\rho 0}\frac{\partial \eta}{\partial x_1} - \frac{g}{\rho 0}\int_{x_3}^{n}\frac{\partial \rho'}{\partial x_i}\partial x_3 + \frac{\partial}{\partial x_j}\left(\nu\frac{\partial u_i}{\partial x_j}\right) - 2\varepsilon_{ijk}\Omega_j u_k \tag{3.1}$$

$$\frac{\partial u_1}{\partial x_1} + \frac{\partial u_2}{\partial x_2} + \frac{\partial u_3}{\partial x_3} = 0 \tag{3.2}$$

where u_i is the velocity vector components in the cartesian x_i direction, ν is the turbulent viscosity, η is the free surface elevation, g is the gravity acceleration, ρ_{atm} the atmospheric pressure, ρ the density and ρ' is anomality, $\rho(\eta)$ is the free surface density, t is the time, h is the depth, Ω is the earth velocity of rotation and ε is the alternate tensor.

The calculation of ρ is obtained as function of water temperature and salinity by the United Nations Educational, Scientific and Cultural Organization (UNESCO) equation of state (Fofonoff and Millard, 1983).

The model transport equation of heat and salt (or any other variable), is given by the advection-diffusion equation:

$$\frac{\partial C}{\partial t} + u_j\frac{\partial C}{\partial x_j} = \frac{\partial C}{\partial x_j}(K\frac{\partial C}{\partial x_i}) + FP \tag{3.3}$$

where C is the property concentration, K the diffusion coefficient and FP is the gain or loss term.

The surface fluxes (importante for the heat transport) are composed by the momentum, sensible heat, latent heat, evaporation and infrared radiation (Chapra, 1997). The wind stress is calculated according to Equation 3.4:

$$\tau_w^u = \rho_a C_a u_{10}\sqrt{u_{10}^2 + v_{10}^2} \tag{3.4}$$

where τ_w^u is the surface stress induced by the wind, ρ_a the air density, u_{10} and v_{10} are the horizontal components of the wind measured at 10 m height above sea surface and C_a is the drag coefficient (Riflet, 2010).

The model horizontal discretization is performed using an Arakawa C grid (Arakawa,

1966), while for the vertical coordinate an hybrid and generic scheme, which allows to choose between z-level, sigma and lagrangian coordinates (Martins *et al.*, 1998; Riflet, 2010).

3.2 Model implementation

As previously referred, two model implementations were used throughout this thesis. Both applications are composed by nested grids and follow the downscaling methodology used by Leitão *et al.* (2005) and Vaz *et al.* (2011).

The applications use three levels of one-way nested grids with different resolution. The estuarine model is a full 2D application that runs offline and is used to calculate the exchange flow between the Tagus estuary and the adjacent coastal area, while the coastal model is a full 3D application used to compute the propagation of the estuarine discharge on the coastal region.

3.2.1 Tagus Estuary model

The estuarine model implementation follows the procedure developed by Vaz *et al.* (2011) and Silva (2012). They present a 2D nested implementation with three domains (Figure 3.1). The first domain (E1) covers the Atlantic coast of the Iberian Peninsula and Morocco and is a 2D barotropic tidal model that is forced at the open ocean boundary with the tidal solution from the Finite Element Solution 2004 (FES2004) model (Lyard *et al.*, 2006). The grid has an horizontal resolution of 0.06º ($\sim$ 6 km). The second domain (E2) is a 2D domain with 0.01º resolution, covering the West coast of the central and southern regions of Portugal. Finally, the third domain (E3) is composed by 335×212 cells with variable horizontal resolution (0.01-0.002º) covering all the Tagus Estuary and the adjacent coast.

Freshwater discharges from the Tagus, Sorraia and Trancão rivers, were imposed at E3 land boundary, obtained from APA website (snirh.pt). Atmospheric forcing was imposed, in all E3 domain, using data from the EMG station. The models time step was 180 s, 60 s and 15 s for E1, E2 and E3, respectively. Further description is available in the Table 3.1.

The estuarine model has been validated by Vaz *et al.* (2011), using harmonic analysis results of measured and predicted sea surface elevation in 12 stations along the estuary. The results of the validation show a deviation lower than 5% of the local tidal amplitude for most of stations, with an average difference of 5º in phase for the main constituent M_2.

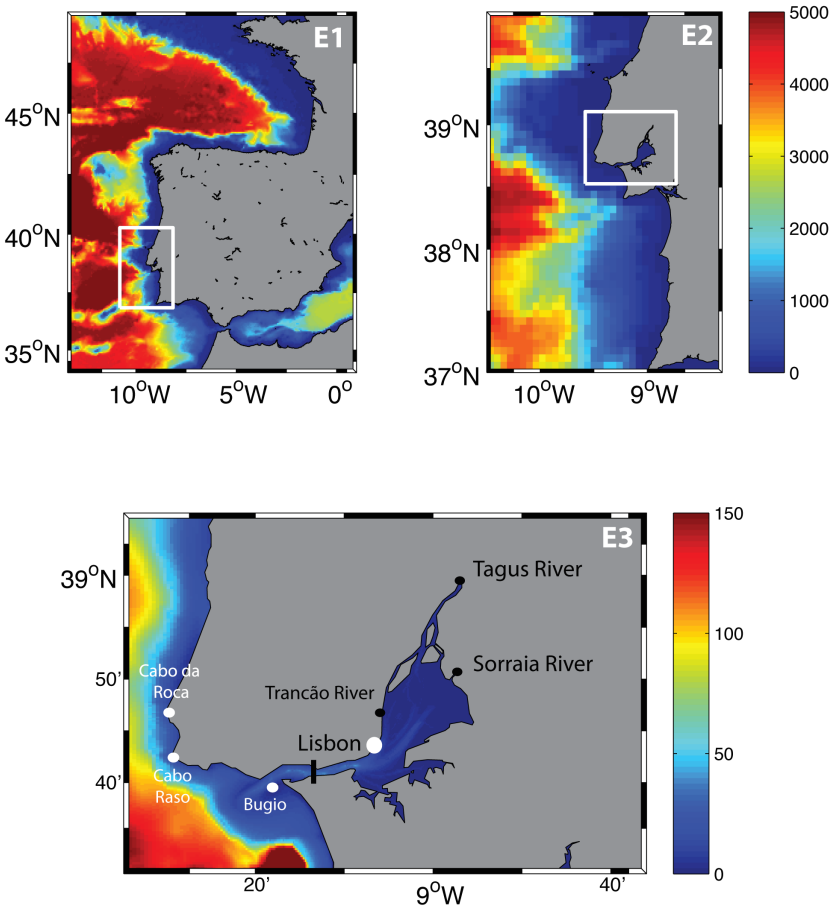

Figure 3.1: Numerical bathymetries used in each domain of the estuarine model, with depth in meters relative to the hydrographic null.

Consequently, the implementation of this model was considered to be able to reproduce the main patterns of the Tagus estuarine circulation.

The estuarine model was used to calculate the exchange flow between the estuary and the near shelf that will be used as landward boundary condition for the coastal model.

Table 3.1: Summary of the estuarine MOHID application.

Domain	**E1 Iberian Peninsula**	**E2 Central Portuguese West Coast**	**E3 Tagus Estuary**
Grid Corners	Lon: -13.5-1.0ºE Lat: 33.5-49.9ºN	Lon: 10.5-8.5ºW Lat: 36.0-39.9ºN	Lon: 9.6-8.7ºW Lat: 38.5-39.1ºN
Dimensions	273 × 241	235 × 122	212 × 335
# of cells	65793	28670	71020
Δx (°)	0.06	0.01	0.01-0.001
Δt (s)	180	60	15
Tide	FES2004	E1	E2
Atmosphere	-	-	EMG
Discharge	-	-	Tagus, Sorraia and Trancao rivers

3.2.2 Coastal model

The coastal implementation used in this work follows the procedure developed by Vaz *et al.* (2009b) and uses three nested domains to compute circulation, heat and salt transport in the region off the Tagus Estuary (Figure 3.2).

The first domain (D1) represents the entire Portuguese continental coast (10.5ºW, 36.6ºN and 6.1ºW, 43.9ºN), and is a 3D baroclinic model based on PCOMS model (Mateus *et al.*, 2012) with an horizontal resolution of 0.06º (∼ 6 km) and 50 vertical layers (7 sigma + 43 Cartesian until the bottom). The second domain (D2) works as a 3D downscaling level with 0.02º (∼ 2 km) of horizontal resolution, representing the region between *Sines* (37.6ºN) and *Figueira da Foz* (40.4ºN). At last, the third domain (D3) represent the region of the Tagus estuary with a spatial horizontal resolution of 0.005º (∼ 500 m) between 38.2º and 39.5º N.

The model D1 gives the SSE, u, v and w velocity components, salinity and water temperature to model D2, which is a 3D baroclinic model with 47 vertical layer used to downscale the solution to the coastal model D3, which is used to compute the propagation and main features of the Tagus estuarine plume. D3 is a baroclinic model with 46 vertical layers (7 sigma layers on the first 8.7 m and Cartesian coordinates from this depth to the bottom).

Additionally, the atmospheric forcing for D1 was provided by the MM5 atmospheric model forecast, with a spatial resolution of 9 km interpolated for the circulation model grid

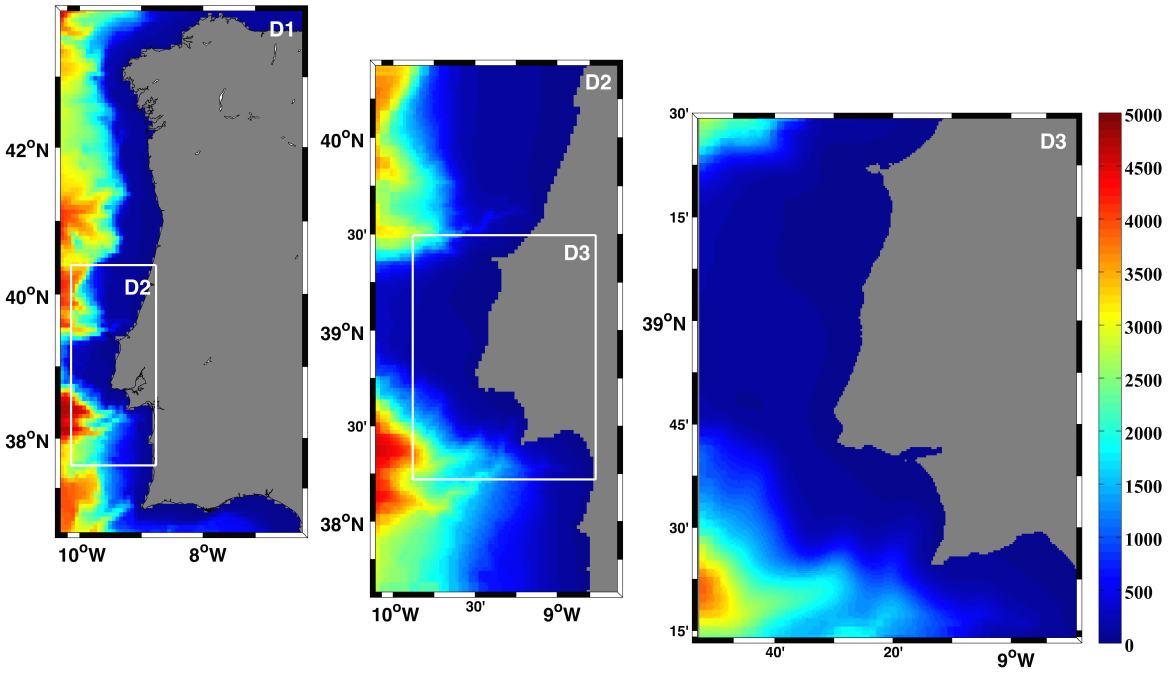

Figure 3.2: Numerical bathymetries used in each domain of the coastal model, with depth in meters relative to the hydrographic null.

(Sousa, 2002; Trancoso, 2012).

The bathymetry of D1 is based on SRTM 30" topo-hydrographic database. D2 and D3 grids are based on the grids from ETOPO1 and GEBCO topo-hydrographic data. D3 numerical grid also uses other high-resolution available data for the estuary mouth. See Table 3.2 for summary of the coastal implementation. The model time step is 180 s, 60 s and 15 s for D1, D2 and D3, respectively.

The atmospheric forcing that was imposed in the D2 and D3 domains is predicted from the WRF model run by the Núcleo de Modelação Estuarina e Costeira (NMEC) (Rodrigues *et al.*, 2015). The data were composed by hourly outputs of air temperature, relative humidity, solar radiation and wind speed, with spatial resolution of 2 km.

At the D3 landward boundary, water exchange with the estuary is imposed, using the calculated output from in the Tagus Estuarine model application.

Table 3.2: Summary of the coastal MOHID application.

Domain	**D1 Portuguese Coast**	**D2 Central Portuguese West Coast**	**D3 ROFI**
Grid Corners	Lon: 10.4-6.2ºW Lat: 36.6-43.9ºN	Lon: 10.1-8.8ºW Lat: 37.6-40.4ºN	Lon: 9.8-8.7ºW Lat: 38.2-39.5ºN
Dimensions	122 × 72	140 × 70	256 x 224
# of cells	8784	9800	57344
Δx (°)	0.06	0.02	0.005
Δt (s)	900	60	15
Z layers	7 Sigma + 43 Cartesian	7 Sigma + 40 Cartesian	7 Sigma + 39 Cartesian
Open boundary	PCOMS	D1	D2
Water Properties	PCOMS	D1	D2

3.3 Validation

Model validation is defined as the procedure where the model outputs are compared with *in situ* measurements to prove the ability of the model in reproduce observations trends or patterns. Qualitative and quantitative analysis will be realized for SSE, u and v components of surface current, temperature and salinity.

In this study, two different water statistical parameters will be calculated, following the procedure by Dias and Lopes (2006). The parameters are:

- **RMSE** - the root mean squared error calculates the absolute measure of the model deviation from data, being one of the most used error parameter to assess tidal model performance (Dias and Lopes, 2006; Oliveira *et al.*, 2006):

$$RMSE = \left\{ \frac{1}{N} \sum_{i=1}^{N} [X_{obs} - X_{model}]^2 \right\}^{\frac{1}{2}} \tag{3.5}$$

  where N corresponds to the number of records and X_{obs} and X_{model} represent observed and calculated data, respectively. For local comparison of SSE, values between 5 and 10 % should be considered very good (Dias *et al.*, 2009).

- **SKILL** - predictive skill from Willmott (1981) overcomes the sensitivity of correlation

statistics to differences in predicted mean and variances (Legates and McCabe, 1999; Warner *et al.*, 2005; Dias *et al.*, 2009):

$$SKILL = 1 - \frac{\Sigma \left| X_{model} - X_{obs} \right|^2}{\sum \left(\left| X_{model} - \bar{X}_{obs} \right| + \left| X_{obs} - \bar{X}_{obs} \right| \right)^2} \tag{3.6}$$

where values of 1 correspond to a perfect adjustment between predictions and observations, while values of 0 indicates a complete disagreement. Higher values than 0.95 should be considered excellent (Dias *et al.*, 2009).

The validation was performed using different datasets. SSE validation was performed using water elevation measurements from the Cascais tide gauge. Surface currents are from an HF radar of the Portuguese navy installed to cover the region near the mouth of the Tagus Estuary, confining the "discharge bay". Salinity and water temperature observations are from the AQUA-MODIS remote sensor.

In this study the SSE predictions from the model D3 was compared with observations of the Cascais's tide gauge. A period of 31 days, between 3-July-2012 and 3-August-2012 was simulated and were used two distinct approaches to evaluate the results: time series and harmonic constituents comparison.

Data from coastal HF radar have increased surface information on coastal currents. The project SIMOC (http://www.hidrografico.pt/simoc.php) maintained by the *Instituto Hidrográfico* (IH), is responsible for two radars in the study region, located in *Forte de São Julião da Barra* (38º 40'N, 9º 19'W) and *Cabo Espichel* lighthouse (38º 24'N, 9º 12'W). The HF radar follows the implementation of the Sines radar (Fernandes and Agostinho, 2008) and works at a 12 MHz frequency with a spatial resolution of 1.4 km. Radar data are obtained in a irregular grid covering all the region near the Tagus Estuary mouth, with a hourly time step. Circulation model predictions were interpolated to the radar data grid, with the same time step. According to Stewart and Joy (1974) and Sentchev *et al.* (2013), for a 12 MHz frequency, the radar measures correspond to the integration of the first meter of the water column.

3.3.1 Satellite data

The use of remote sensing imagery (i.e. MODIS ocean colour data) of SST is a valuable tool in the observation of large-scale oceanic processes. Furthermore, the spatial high-resolution of these images ($\sim$ 1 km) are useful to the validation of heat transport models.

The remote sensing data used in this study was obtained from the MODIS sensor, a key instrument onboard of the Aqua (EOS PM) satellites. MODIS sensor acquires data in 36 spectral bands in a 2300 km wide swath with a nadir nominal resolution of 1000 m (Nishihama *et al.*, 1997). The data used here were Level2 (Lv2) products available at Oceancolor website (http://oceancolor.gsfc.nasa.gov). The long-wave SST product used was obtained applying an algorithm that uses the MODIS 31 and 32 bands at 11 μm and 12 μm. In each image the sensor performs a quality evaluation of the remote data. A quality flag of 0 indicates best quality while 4 indicates complete failure. therefore, for the analysis comparison all pixels with quality flags higher than 1 were removed from the images. This threshold was used since a quality flag of 1 can be representative of upwelling events (low temperatures of SST not expected in the sensor climatology), high river discharge or even clouds (NASA, 2015).

Salinity is a natural tracer for river plumes, but, in coastals region remote sensing imagery do not provide good resolution. For this variable several studies have identified a significant correlation between the surface salinity and turbidity (Valente and da Silva, 2009; Mendes *et al.*, 2014; Fernández-Nóvoa *et al.*, 2015), based on the diference of optic properties from the estuarine discharge to the ocean waters.

The identification of the Tagus estuarine outflow was performed using as proxy the high reflectivity plume waters, which are probably justified by the existence of suspended particulate matter in it. Taking advantage of the available radiance bands in Lv2 product, diverse tests were performed using the bands in 483-672 nm range. The most suitable for this study was the 555 nm (nLw555) radiance band, which is consistent with the results from Nezlin and DiGiacomo (2005) and Mendes *et al.* (2014) for their studies on San Pedro Shelf (southern California) and Douro estuarine plume, respectively.

The evaluation of the water temperature and turbidity from the model was performed using a period from July to December of 2012, which was concurrent with the HF Radar observations.

3.4 Atmospheric model

As previously referred, wind stress plays a key role on the spreading of estuarine plumes, therefore a proper meteorological forcing condition should be taken into account for an accurate reproduction of the water-air interaction (e.g. costal circulation and hydrography).

For the study region there are no high resolution atmospheric data available, being

difficult to successfully force the circulation model and present accurate results. Also, the orography of the *Serra de Sintra*, which acts as a natural wall to the northern wind propagation generating a "shadow" effect to the estuary mouth, can produce misleading results regarding coastal hydrography and circulation as pointed out by Vaz *et al.* (2015). Therefore, in order to overcome this difficulty was implemented an atmospheric model for the study area, with 2 km of spatial resolution. For this purpose, and in the frame of this work, was implemented for the region under study the Weather Research and Forecasting model (WRF) version 3.6.1 (Skamarock *et al.*, 2008). This model has being widely used, not only by researchers, but also by institutions as national meteorological institutes (Pereira *et al.*, 2013). The implementation developed uses three two-way nested domains. The downscaling methodology follows a domain ratio of 1/3, with the father domain (WRF1) covering most of the Iberian Peninsula with a spatial resolution of 18 km. The two other domains (WRF2 and WRF3) present 6 and 2 km resolution, respectively (Figure 3.3).

The atmospheric model boundary condition is predicted each 6 hours by the Global Forecast System (GFS) model (NCEP, 2003) with 1º spatial resolution. The vertical discretization was composed by 28 unequal spaced layers at each domain.

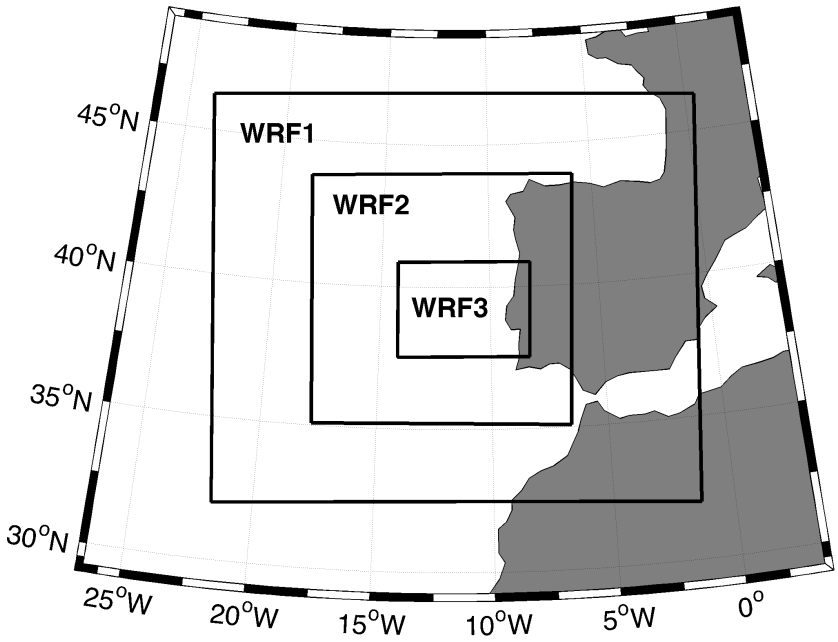

Figure 3.3: Nested domains used for atmospheric simulations.

3.4.1 Validation of the WRF model

Aiming to validate the meteorological model outputs, was performed an assessment of the WRF3 model. Model predictions of air temperature, wind intensity and direction were compared with EMG station measurements (Figure 2.4). The visual assessment of the model results revealed that it can accurately reproduce the general variability of the data (for both variables). Then a quantitative evaluation was performed comparing the model predictions and the EMG station observations. The EMG station is located near *Cascais*, a very urbanized area, situated south of *Serra de Sintra*.

The wind intensity and direction are two important variables to characterize the atmosphere dynamics. However, they are difficult to predict with accuracy, especially at the Lisbon Bay due the existence of *Serra de Sintra*. From Figure 3.4 is noticeable that model overestimates wind intensity, presenting RMSE values of 4.89 ms^{-1} (27% of the local wind intensity amplitude). For the wind direction, the model presents better performance (RMSE of 41.8º (13.4% of the local amplitude)), which reveal an adequate reproduction of the temporal patterns. Some discrepancies could be attributed to the fast changes induced by maritime breeze in this area (Alcoforado and Lopes, 2003).

Concerning the air temperature predictions, the WRF outputs show a SKILL score of

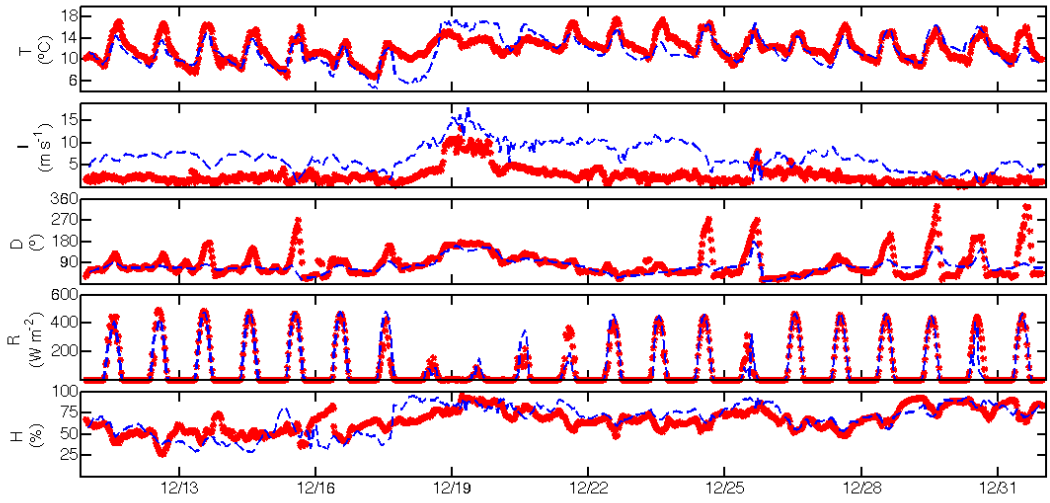

Figure 3.4: Variability of WRF3 data and EMG station data for temperature (Temp), wind intensity (Int) and direction (Dir), humidity (Hum) and radiation (Rad) for 10-31th of December 2007. Red line represents EMG station data and the the blue line the WRF3 predictions.

0.83 with a RMSE of 1.91°C (17.5% of the local amplitude). Regarding solar radiation and relative humidity a very good correlation between *in situ* data and model predictions was computed, with SKILLS of 0.97 and 0.82, respectively. Full quantitative assessments are presented on Table 3.3.

The atmospheric model implementation was considered successfully validated for the study region. The results show that the model is able to accurately reproduce the main atmospheric features of this region, being able to produce accurate boundary conditions for the coastal model.

Table 3.3: Quantitative assessment of WRF model predictions with EMG station observations for the period of 10-31th of December 2007.

	Temp (°C)	**Int (ms^{-1})**	**Dir (°)**	**Rad Wm^{-2}**	**Hum (%)**
RMSE	1.91	4.89	32.42	9.57	18.18
SKILL	0.83	0.48	0.73	0.97	0.81

3.5 Wind patterns assessment in the Tagus region

The influence of the wind stress on the surface of the ocean has a large impact on surface current variability. This is quite true in estuarine plume propagation studies. The adjacent coast of the Tagus Estuary is highly influenced by the wind variability. For that reason a seasonal assessment was performed in order to identify the dominant wind patterns, in terms of more frequent and significant wind directions and intensity.

The wind characterization was performed through the analysis of data from the meteorological station of the Lisbon airport (Figure 2.4). This station is located in the middle of the city presenting one of the longer time series of data in the region, and can be considered representative of the wind patterns in the study region. The available data comprises the period from 2001 to 2007.

The events were splinted following the Beaufort wind force scale that relates the wind speed to observed conditions at sea. The statistics of wind intensity and direction (Table 3.4) has identified the probability of calm winds (bellow 1.5 ms^{-1}) to be near 8.1%. Light, gentle and moderated breezes present similar percentages, corresponding to a total of 84.6% and in only 7.3% of the cases the wind is higher than 8 ms^{-1}.

Table 3.4: Percentage of events observed in each range of wind speed according to Beautfort scale for the airport station for the period between January 2001 and December 2007.

Wind Limits (ms^{-1})	**Beaufort Scale description**	**General**	**DJF**	**MAM**	**JJA**	**SON**
less then 1.5	Calm	8.1	11.5	6.4	3.7	11.1
1.5 - 3.3	Light breeze	30.2	36.0	28.4	20.4	36.5
3.3 - 5.5	Gentle breeze	34.4	34.0	34.8	35.3	33.6
5.5 - 8.0	Moderate breeze	20.0	13.7	22.5	28.8	14.5
8.0 - 10.8	Fresh breeze	6.0	3.6	6.6	10.2	3.4
more then 10.8	Strong breeze	1.3	1.2	1.2	1.6	0.8

The seasonal variability was evaluated in order to identify the main wind direction for each season. The original data was divided in winter (DJF - December, January and February), spring (MAM - March, April and May), summer (JJA - June, July and August) and autumn (SON - September, October and November) and wind roses for each season are presented in Figure 3.5.

During winter, the dominant direction is from NE with about 20% of the occurrence, followed by NNW direction with 12% of occurrences (Figure 3.5a). 80% of the wind intensity was lower than 5.5 ms^{-1}.

Spring season shows a strong influence (37%) of winds from NW and NNW (Figure 3.5b). The wind intensity increases comparatively to the winter, with less than 70% of the cases below 5.5 ms^{-1}. Strong winds from the N-NW quadrant were identify in the region.

The Summer season results are very similar to the spring results (Figure 3.5c). Here energetic winds with over 40% of observations higher than 5.5 ms^{-1} are observed. The major predominant directions are: NW and NNW with 30% and 28% of occurrences, respectively.

Autumn season presents a similarity with the winter season, specially in intensity. More then 80% of the observations show a wind intensity lower than 5.5 ms^{-1} (Figure 3.5d).

The previous results are similar to those obtained by Angi (2011) and Lopes *et al.* (2013). Moreover, Alcoforado (1987) has identified about 45% of the days with predominant northern winds.

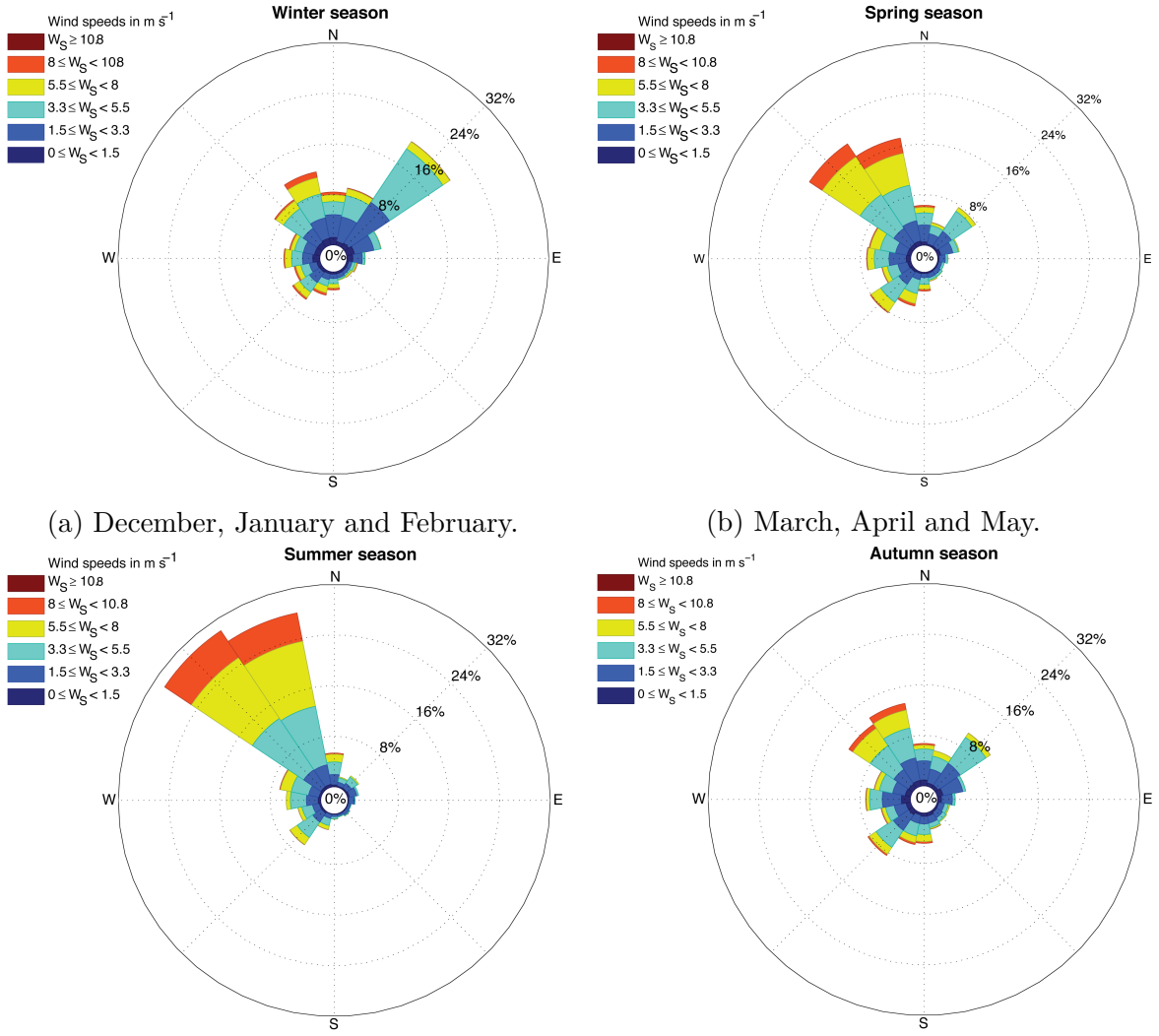

(a) December, January and February.

(b) March, April and May.

(c) June, July and August.

(d) September, October and November.

Figure 3.5: Wind roses calculated for (a) winter, (b) spring, (c) summer and (d) autumn, from meteorological airport station data, for the period between January 2001 and December 2007.

3.6 Self-Organizing Maps

In order to analyse the model predictions, a new method based on a neural network is used to study the region surface variability. The method is similar to a classic EOF analysis, but presents more effective results on the computation of coastal variability (Liu *et al.*, 2006b)

The Kohonen's Self-Organizing Map (SOM) is an Artificial Neural Network (ANN) that have the capacity of learning without supervision. This algorithm was developed in the

early 80's of the XX century by Kohonen (1982) during the research of auto-associative memory. Here, the SOM as *"visualization and analysis tool for high dimensional data"* is described. Moreover, the algorithm can be used for clustering, dimensional ordering and reduction, classification and sampling (Lobo, 2009).

The SOM analysis was performed using the SOM Toolbox 2.0 (Vesanto *et al.*, 2000). This toolbox was generated for MATLAB® being maintained by the Helsinki Technical University. It is a freely available on the institution website (http://www.cis.hut.fi/).

To perform a SOM analysis, each data series was reshaped to a row vector forming a 2D matrix (data array). At each interaction, the row vectors are used to update the weight of the SOM via an unsupervised learning algorithm. The final weight vectors are then reshaped back to the original grid and provide different data patterns depending on the mapping requested (illustrative of SOM working system in Figure 3.6).

This training is an interactive process. At each training step one sample vector $\mathbf{x}$ from the input data set will be chosen randomly and the distance between it and all the weight vectors will be calculated. The calculation follow the Euclidian distance method, where the closer neuron to the input vector $\mathbf{x}$ is the wining neuron, called Best-Matching Unit (BMU).

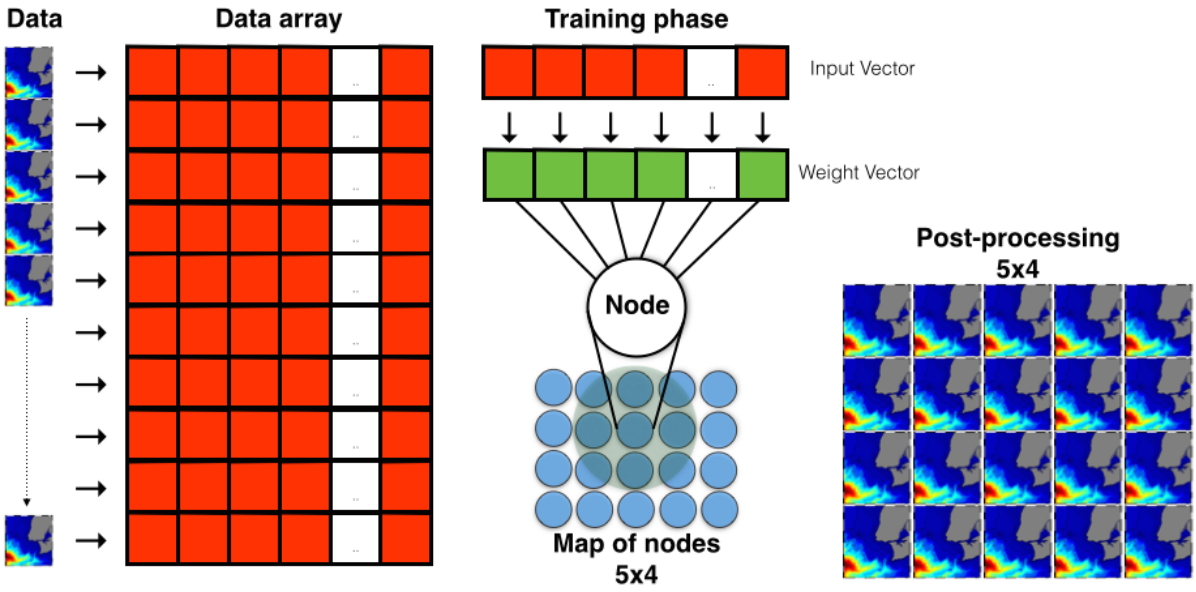

Figure 3.6: Schematic illustration of SOM organizing system (adapted from Richardson *et al.* (2003)).

The toolbox BMU calculation follows the procedure from equation 3.7:

$$\|\mathbf{x} - \mathbf{m}_c\| = min\{\|\mathbf{x} - \mathbf{m}_i\|\} \tag{3.7}$$

where $\|.\|$ represents the distance measure. The toolbox has improved from the original code, introducing interpolation of missing values and mask for excluding certain variables.

After the identification of the BMU, the SOM weight vectors are updated moving the BMU closer to input vector. This leads to a stretching of the BMU and is topological neighbours in direction of the vector sample. The calculation of unit i weight vector follows equation 3.8:

$$\mathbf{m}_i(t+1) = \mathbf{m}_i(t) + \alpha(t)\varepsilon(t)[\mathbf{x}(t) - \mathbf{m}_i(t)] \tag{3.8}$$

where t stand for time, $\mathbf{x}$(t) is a random input vector from input data set at time t, ε the neighbourhood kernel around the winner c and α the learning rate for the snapshot t.

The training of SOM is usually performed in two phases: the first one, using a high learning rate and neighbour radius; in the second phase, both of the previous parameters are set for small values right from the beginning of evolution calculus. This action leads the first training of the SOM to reproduce the same space of the input data and then adjust the previous information's improving the training map (Vesanto *et al.*, 2000).

3.7 Scenarios description

Once the coastal model is validated, it may be used to assess the impact of several scenarios of river inflow and wind in the Tagus estuarine plume propagation, namely in salinity and water temperature variability.

In order to study the region variability, a set of scenarios were designed and the effect of the wind and river inflow in the coastal hydrography studied (Figure 3.7).

In this study three scenarios were simulated: Scenario A (ScA) considered as reference, composed by discharge and wind forcing, Scenario B (ScB) without wind forcing and Scenario C (ScC) without Tagus estuarine discharge. In each scenario three distinct Tagus River discharges (Figure 3.8) were implemented: 1500 m^3s^{-1} (Discharge1) and 3000 m^3s^{-1} (Discharge2) representative of the 90 and 99 percentile results of the long discharge series analysis, respectively, and a 5000 m^3s^{-1} (Discharge3) river discharge representative of a high discharge event registered in March-April of 2013. The scenario

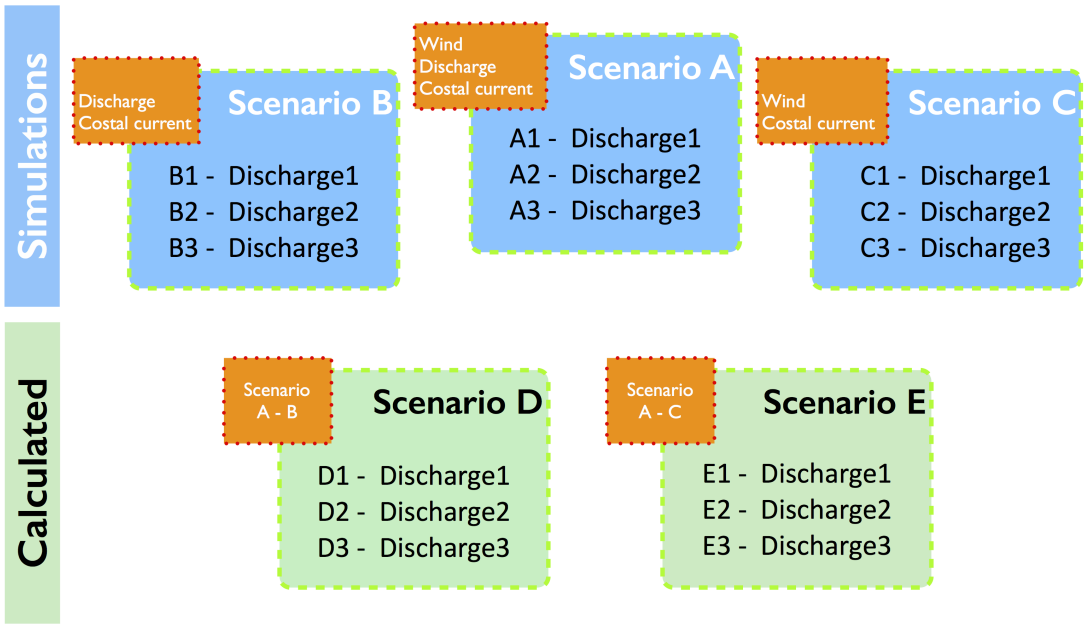

Figure 3.7: Scheme of the scenarios implementation.

simulation was performed for a 23 days period, starting in 8 November of 2012.

Two new scenarios were calculated from scenarios A to C. Scenario D (ScD) results from the difference of ScA and ScB while Scenario E (ScE) results from the difference of ScA and ScC, aiming to understand the influence of wind and river inflow, respectively.

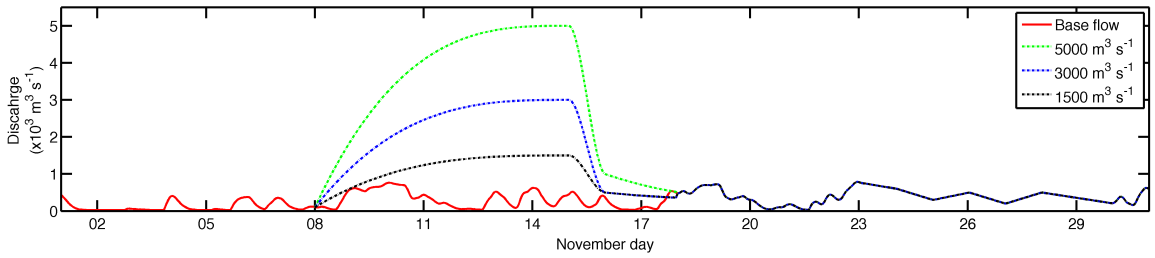

Figure 3.8: Tagus river discharge used in each scenario.

Chapter 4

Results and Discussion

4.1 Model validation

The estuarine model used in this study was previously implemented by Vaz *et al.* (2011) and used to study circulation and hydrography features of the Tagus Estuary (Vaz *et al.*, 2011; Silva, 2012). More details on the model's implementation can be found in these studies. Therefore, the results presented in this section are only related with the coastal model validation procedure.

4.1.1 Sea surface elevation

SSE from the model was compared with data from the Cascais tide gauge, in order to evaluate the model skill in reproducing water elevation in the coast near the Tagus mouth (Figure 4.1).

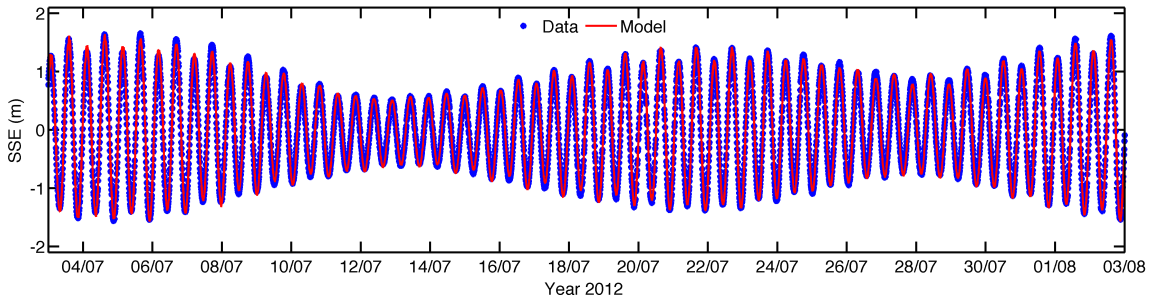

Figure 4.1: Predicted (−) and observed (•) normalized SSE (m) for Cascais tide gauge used in the validation of the coastal application.

The predicted SSE follows the observed records, with a root mean squared error (RMSE) and SKILL of 0.33 m (9.8% of relative error to local observed amplitude) and 0.96, respectively, revealing the model's accuracy in reproducing the tidal wave propagation in the region near Tagus mouth.

In order to quantify the main differences between model predictions and observed data, a comparison of the amplitudes and phases of the main solar (K_1, O_1, Q_1) and lunar (M_2, S_2, N_2) constituents was performed using the harmonic analysis software *T_Tide* (Pawlowicz *et al.*, 2002). A 31 days time series of hourly observed and predicted SSE data was used (Table 4.1). The overall distribution of the observed and predicted amplitude and phase are similar. The M_2 and S_2 constituents are responsible for more than 80% of the tidal energy. M_2 presents an amplitude error of 0.5 cm and a phase lag of 3.4 (about 7 minutes), while for S_2 the amplitude error was 0.4 cm with a lag of 4.5º (about 9 minutes). For the diurnal constituents the amplitude errors range from 0.3 to 1.4 cm and for the phase errors between 0.6 and 26.5º, respectively. The tide is semi-diurnal, with a Form Number (FN) of 0.14 (Defant, 1960).

In general, the harmonic analysis results show that the circulation model reproduces well the tide amplitude and phase.

Table 4.1: Difference of harmonic constituents, amplitude (cm) and phase (°) for the main tide constituents. Analysis period between 03-July and 8-August 2012.

	Amplitude (cm)			**Phase (°)**		
	Data	**Model**	**Diference**	**Data**	**Model**	**Diference**
M_2	98.9	99.4	-0.5	94.4	97.8	-3.4
S_2	32.2	31.8	0.4	135.3	139.8	-4.5
N_2	19.3	19.5	-0.2	69.5	71.5	-2.0
K_1	8.6	7.2	1.4	79.4	52.9	26.5
O_1	5.9	5.6	-0.3	328.4	332.2	-3.8
Q_1	2.1	2.4	-0.3	269.1	269.7	-0.6

4.1.2 Surface current

The model skill in reproducing surface currents was also tested. These are key and challenging validation parameters due to their characteristic high spatial and temporal variability. Here surface water velocity (first meter) from the model was compared with data from the HF radar installed in the region. As a measure of the mean deviation of the

model predictions to the HF radar observations, the RMSE and SKILL were calculated using data of November 2012. For this period, 622 HF radar data fields (of 744 possible) were available. Both error calculations were performed for the zonal (u) and meridional (v) current components, at each radar grid cell.

The mean RMSE value across the region is 14.9 cms^{-1} and 15.9 cms^{-1} for zonal and meridional component, respectively. That is, these values represent relative errors to local amplitude of 22.0 and 17.8% in u and v current components, respectively (Figure 4.2). SKILL assessment for the same period (Figure 4.3), shown a better representation by the circulation model of the v current component, with a mean value of 0.71, while for the u current component, the obtained mean value was 0.52.

HF radar measures could suffer from limitation that may produce erroneous RMS and SKILL values. One of those limitations is the Geometric Dilution of Precision (GDOP), that appears when the angle between two radial vectors is too large to enable accurate resolutions of the component perpendicular to the radial (Chapman *et al.*, 1997; Trujillo *et al.*, 2004; O'Donncha *et al.*, 2015). This limitation could be the reason for the low quality results obtained in the baseline region (line that connect the two HF radar stations), specially for the u current component.

Despite the RMS and SKILL values, those are consistent with studies by other authors.

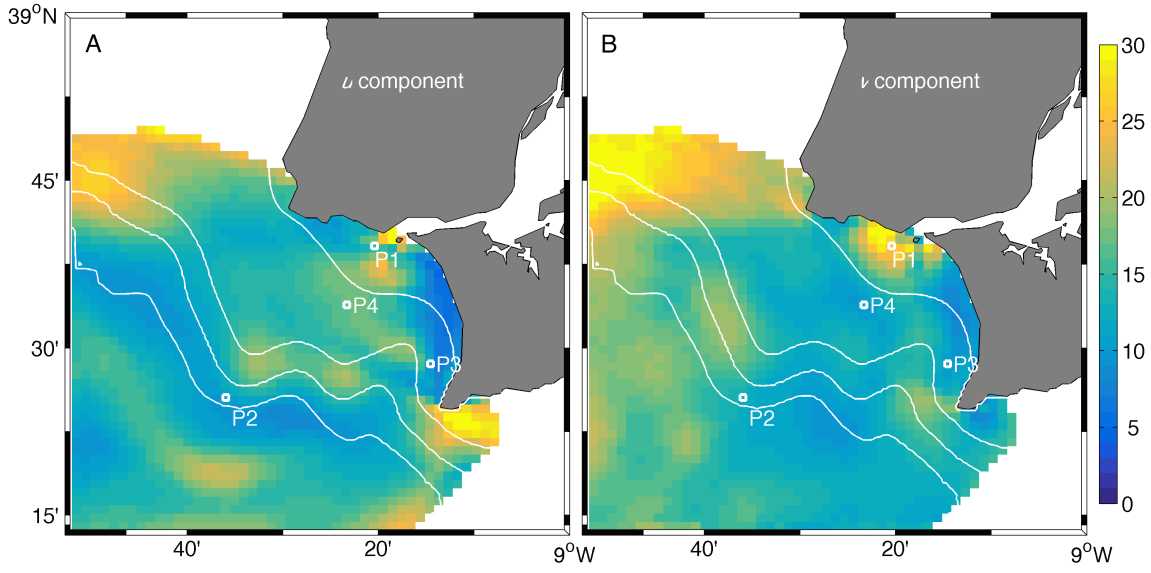

Figure 4.2: RMSE assessment between model simulations and HF radar measure current in (A) zonal and (B) meridional component of velocity. Magnitude of deviation in cms^{-1}.

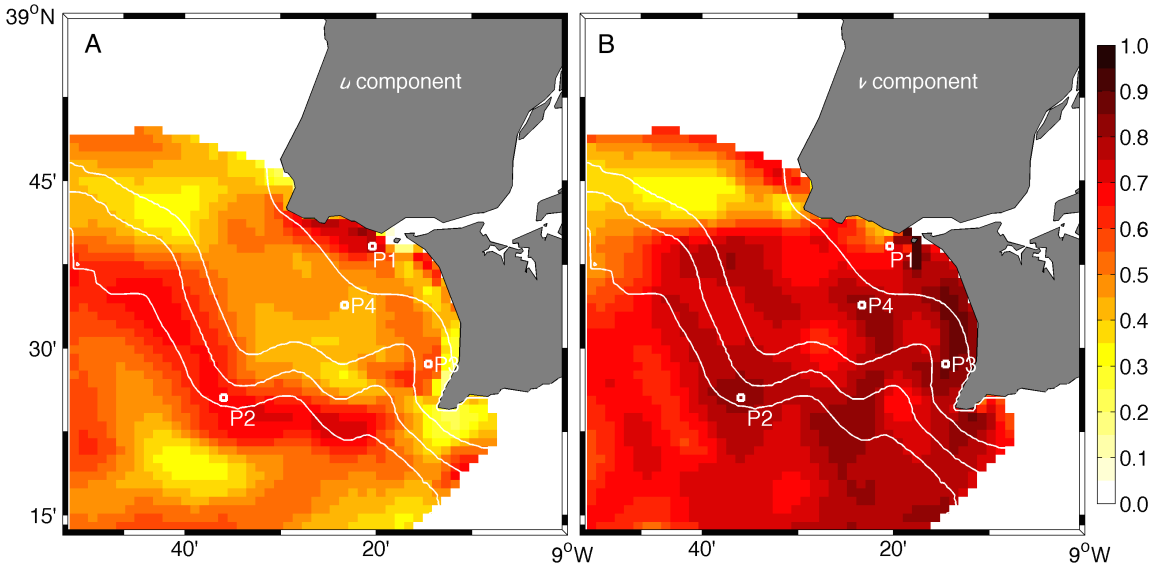

Figure 4.3: SKILL assessment between model simulations and HF radar measure current in the (A) zonal and (B) meridional component of velocity.

In fact, O'Donncha *et al.* (2015) performed a similar study in Galway Bay (Ireland), where they obtained a mean RMSE deviation over 23.8 cms^{-1} with SKILL score of 0.7 (zonal) and 0.56 (meridional) for current velocity.

In order to evaluate the temporal variability of surface currents in the region, and to compare model predictions with radar data at specific points within the plume pathways (Figure 4.3 - P1, P2, P3 and P4), several monitoring points were chosen (Figure 4.4).

In P1 is visible the influence of the tide on both current components. Additionally, the estuary mouth bathymetry presents special features, as the existence of a small island, *Bugio*. For that region, a circulation model using a grid of 500 m could not be enough to fully describe the circulation here, the RMS error is 18.2 and 20.7%, respectively. Moreover, this region present complex circulation features with two "permanent eddies" (Fortunato *et al.*, 1997; Vaz and Dias, 2014), which can modulate the circulation, turning it less predictable with a 500 m resolution model. However, for other points is found a good reproduction of the observed data, with RMSE values of local amplitude for u velocity component of 18.1, 23.7 and 20.3% and for v velocity component of 12.6, 16.4 and 17.5%, for stations P2, P3 and P4, respectively.

Despite of differences, the model predictions can describe the spatial and temporal variability of surface currents, therefore, was considered validated for the region.

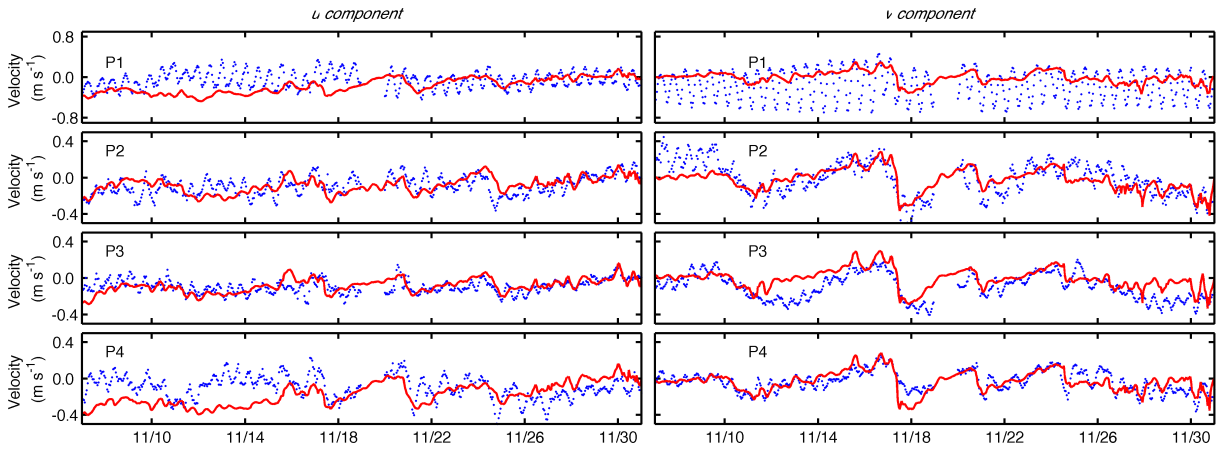

Figure 4.4: Time series overlapping of model predictions (red line) and HF radar surface current components (blue dots), for the points displayed in Figure 4.3. Left column represent zonal component and right column the meridional component of current.

4.1.3 Satellite vs model SST and salinity

Once the circulation model is considered validated, it is necessary to evaluate the transport model. One way to evaluate water temperature and salinity predictions is to compare model outputs with satellite imagery. This would give a spatial assessment of the local patterns for these variables. In this thesis an assessment was performed for the simulation period, from July to December of 2012 (Figures 4.5 and 4.6). Images that present more valid pixels after quality flag cleaning were chosen to compare with model outputs.

Overall deviation of predicted SST comparatively to the remote sensing images shows values under 2ºC. In spite of the low difference value, the objective is the accurate spatial variation reproduction. The model could reproduce the general spatial variability of SST, with higher values found in regions far of the coast, decreasing towards the coast region. Despite the similar patterns found, it is important to highlight the existence of small deviations. Low temperature bands near coast tend to be thinner in the predicted than in the remote sensing data, while offshore high temperature zones, observed in remote sensing images, have lower temperature values in the model predictions.

In order to evaluate salinity surface patterns, images from the MODIS nLw555 were used as plume tracers (Figure 4.6). Low salinity fields resulting from the Tagus Estuary discharge were compared with the high turbidity values. In general, the model could reproduce the spatial pattern of the plume, with the low salinity regions located in the same regions of high turbidity. Under southward winds, remote imagery shows a S-SW propagation of the

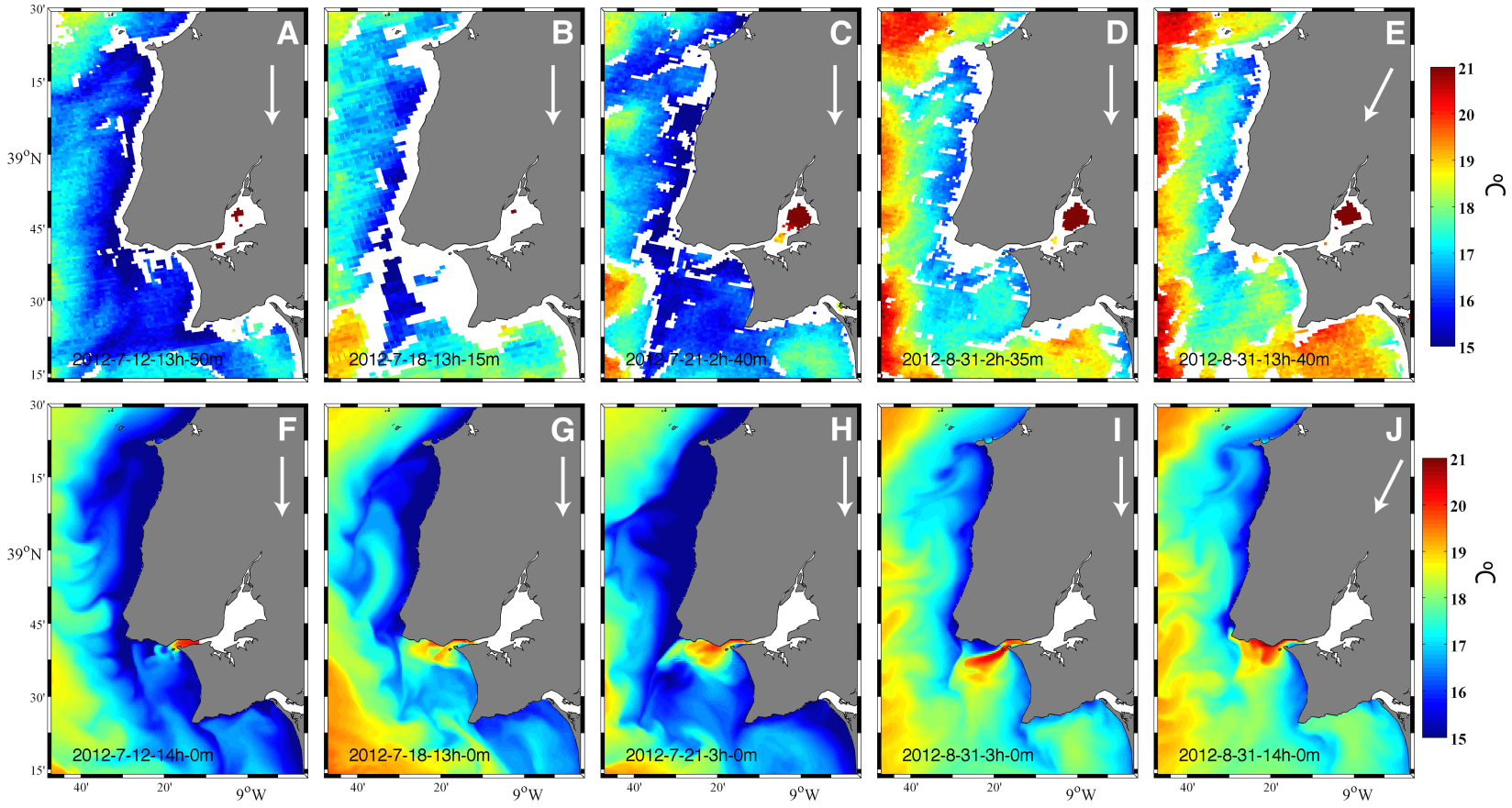

Figure 4.5: Comparison of SST from MODIS sensor (upper row) and circulation model output (bottom row) for the days 12, 18 and 21 of July and 31 of August of 2012. White vectors represent the previous 6 hours mean wind directions.

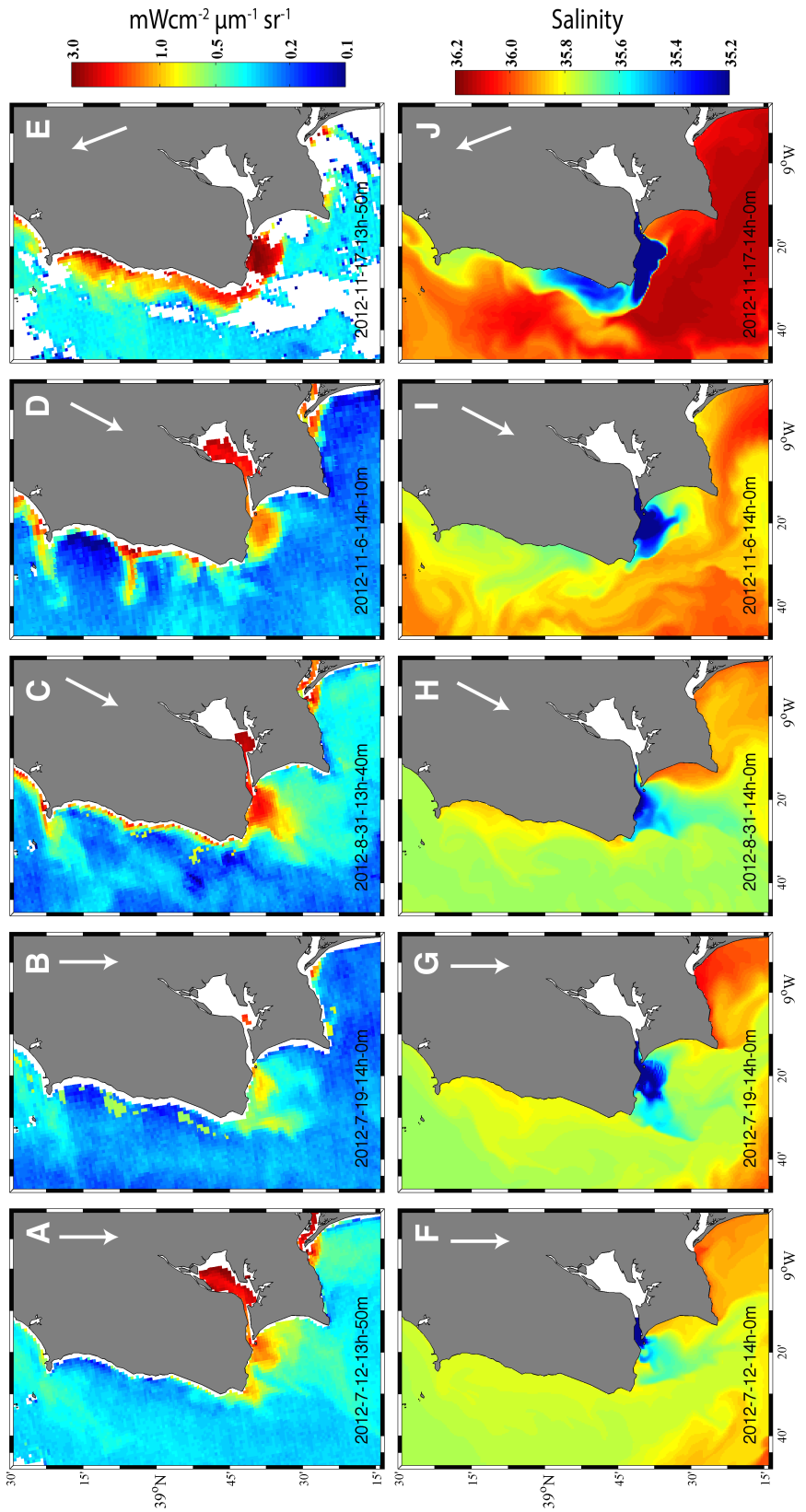

Figure 4.6: Comparison of the turbidity signal from MODIS sensor (upper row) and circulation model surface salinity output (bottom row) for days 12 and 19 of July, 31 of August and 6 and 17 of November of 2012. White vectors represent the previous 6 hours mean wind directions.

plumes followed by the predictions of the transport model (Figure 4.6 - A,B,C - F,G,H). For transitional (Figures 4.6 - D and I) and downwelling winds (Figures 4.6 - E and J), the model predictions of the plume follow the high turbidity values with good accuracy.

Occasionally, high turbidity regions were observed under southward winds. This could be the result of chlorophyll blooms, which may change the optical properties of the waters. Similarly, near the Sado Estuary mouth region (south of *Cabo Espichel*) high turbidity values are observed, resulting probably from the estuarine discharge. However, this estuarine outflow is not implemented on the transport model disallowing their comparison.

Taking into account all the previous results, the transport model was considered validated and, therefore, it can be used to study issues concerning water temperature and salinity local variations.

4.2 Scenarios

4.2.1 Self-Organizing Maps

In this work, the variability of the salinity in the coast off the Tagus Estuary was study using the SOM toolbox. The evaluation of coastal variability was performed using predicted fields of surface salinity from the previously defined scenarios: ScA, ScB and ScC.

The results of the simulation with atmospheric forcing (observed wind intensity and direction, Figure 4.7 - F) and a maximum river discharge of 5000 m^3s^{-1} (ScA-A3, Figure 4.7 - G) are depicted in Figure 4.7. Four nodes were used to reproduce the spatial salinity variability identified by the SOM analysis, in which the Node 1 is representative of the pre-discharge signal, and represents 28.2% of the local variability, while Node 2 is representative of a transitional wind regime, and represents 25.1% of the local variability. Node 3 represents a upwelling favourable wind period after high river discharge (28.5% of the local variability). Node 4 is representative of the high river discharge signal and counts for 18.2% of the total variance of the system.

A BMU number represents each SOM spatial node, at each instant. BMU's time series were sorted by plume size and compared with local wind stress and river discharge time series (Figure 4.7 - E, F and G). The relation between discharge and BMU's time series is well reproduced for the high discharge event observed until day 18, following a BMU sequence of 1-2-3-4-3-2-1. For the rest of the simulation period, the wind stress obtains the higher relation with BMU's 1 and 3, being representative of strong and weak upwelling

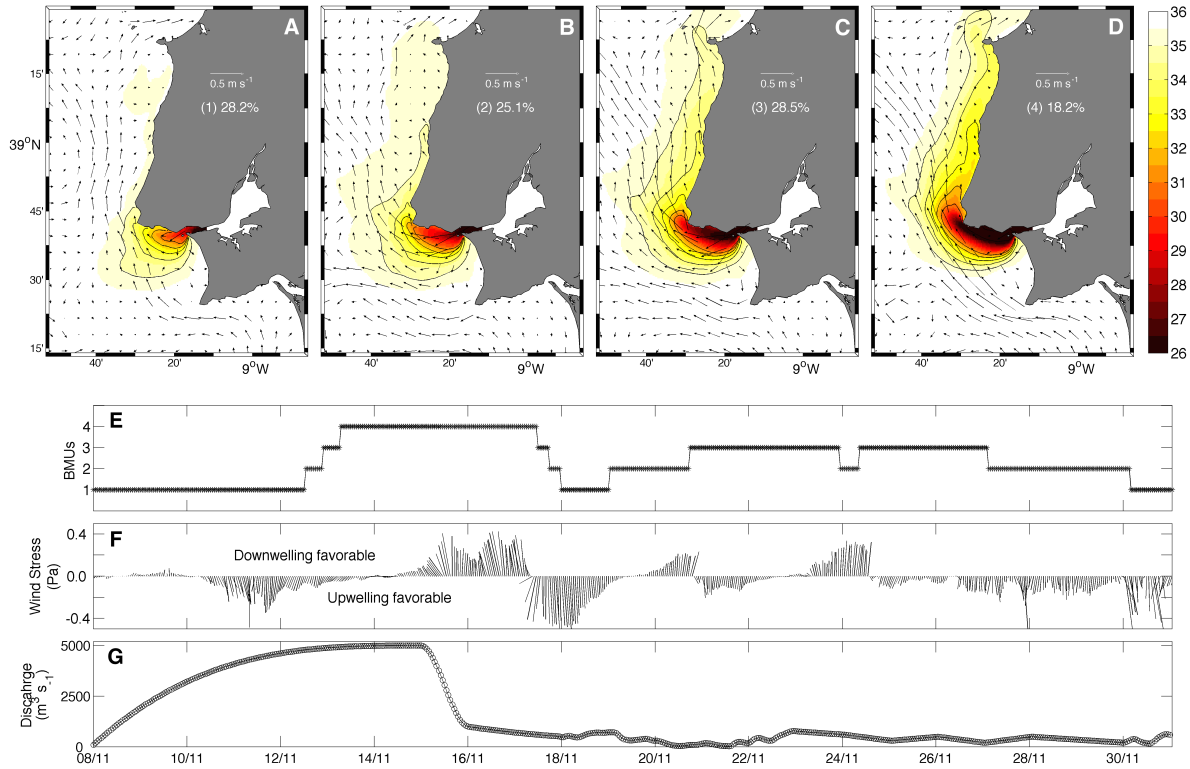

Figure 4.7: A 1x4 SOM representation of the surface salinity field for ScA-A3 for the period of 8-31 of November. Upper panel (A-D) represent the SOM pattern. The frequency of occurrence is shown in the figure, as the surface mean velocity vectors for the period of each BMU. Bottom panel shows time series of (E) BMU, (F) wind stress and (G) freshwater river discharge.

favourable winds, respectively. Under downwelling favourable winds, BMU3 is the most representative.

In Figure 4.8 is depicted the SOM analysis of the ScB-B3 in order to obtain the influence of the freshwater inflow, with a maximum estuarine discharge of 5000 m^3s^{-1} (ScB-B3, Figure 4.8 - F) without wind stress forcing. The four nodes represent the stages of the plume evolution, under high discharge without wind forcing (Figure 4.8 - A, B, C and D). The Node 1 represent the initial state, representing 24.5% of the total variance. Nodes 2 and 3 are the result of the increasing estuarine discharge and represent 12.5 and 19% of the total variability, respectively. The full developed plume resultant of the high river discharge is represented by the Node 4 (44% of the total variance).

From the SOM analysis is visible that all nodes show a surface bulge confined to shore.

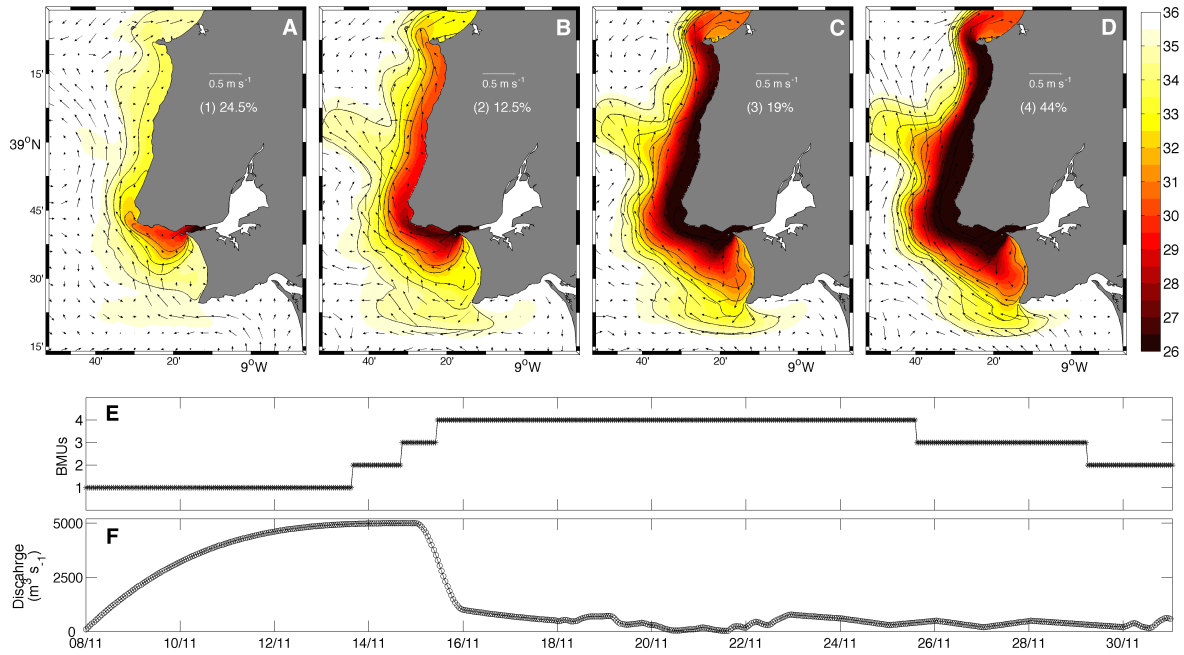

Figure 4.8: A 1x4 SOM representation of the surface salinity field for ScB-B3 for the period of 8-31 of November. Upper panel (A-D) represent the SOM pattern. The frequency of occurrence is shown in the figure, as the surface mean velocity vectors for the period of each BMU. Bottom panel shows time series of (E) BMU and (F) freshwater river discharge.

Similar effects were identified in several studies of surface-advected plumes on the North Hemisphere (Chao and Boicourt, 1986; Chao, 1988; Kourafalou *et al.*, 1996). These authors have concluded that the surface buoyant outflows spread radially from the estuary mouth and are deflected to the right by the Coriolis force.

BMU's time series were ordered by the plume dimension and compared with the river discharge time series (Figure 4.8 - E and F). The relation between series shows a delay in the maximum river discharge and the observation of the BMU4. The BMU's follow the 1-2-3-4 sequence followed by a slow reduction from 4-3-2. The slow reduction of the surface salinity may be the result of the lack of wind mixing and lower transport velocities.

The results of the simulation without estuarine discharge (ScC-C3) to evaluate the wind effect on the plume propagation are represented in Figure 4.9. SOM analysis used four nodes to reproduce the spatial salinity field. Node 1, Node 2 and Node 3 were representative of 16.8%, 14.4% and 10.3% of local variability, respectively, while Node 4 is the dominant node, with 58.5% of the local variability. In all nodes is visible that the salinity variability is controlled by a northward coastal circulation observed during the simulation period, that

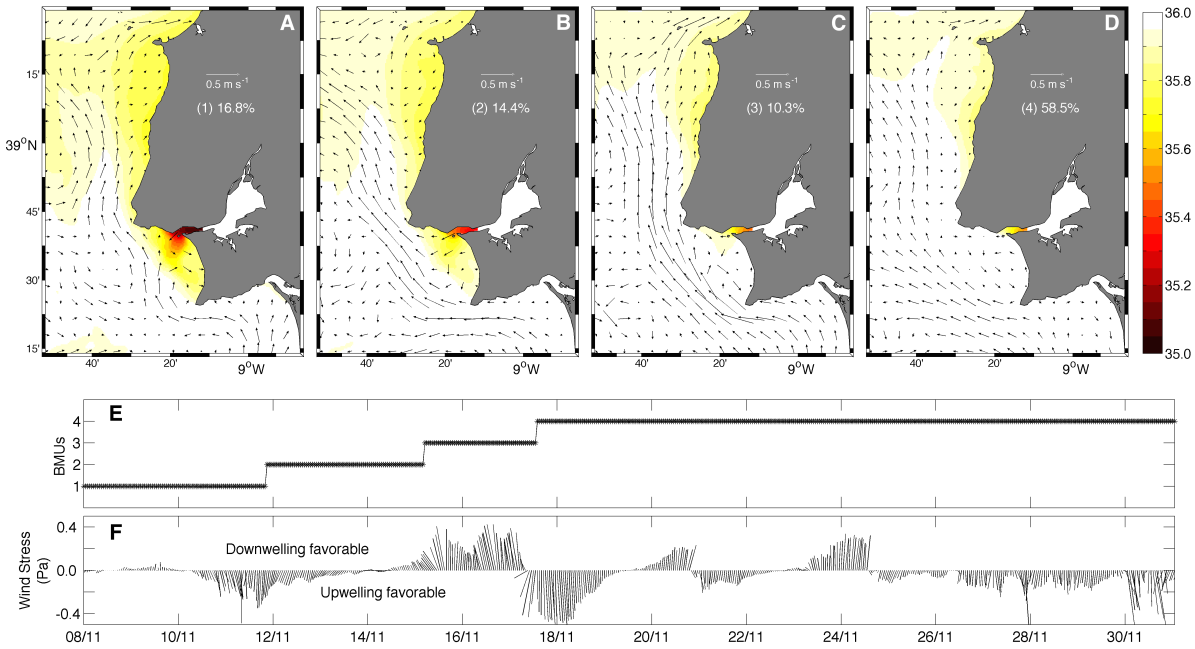

Figure 4.9: A 1x4 SOM representation of the surface salinity field for ScC-C3 for the period of 8-31 of November. Upper panel (A-D) represent the SOM pattern. The frequency of occurrence is shown in the figure, as the surface mean velocity vectors for the period of each BMU. Bottom panel shows time series of (E) BMU and (F) wind stress.

could be the PCCC, observed during the winter months. In the region of Tagus Estuary mouth is observed the salinity signal produced by the period of spin up before the scenario implementation.

Each SOM spatial node was represented by a BMU number, at each instant, being ordered by the dimension of high salinity region and compared with local wind stress time series (Figure 4.9 - E and F). It was not identified a relation between SOM salinity BMUs time series and wind stress. Nevertheless, when performing a relation with the node's surface current was possible to identify that under downwelling favourable winds (Node 3) is observed an increase of the surface current towards north.

4.2.2 Influence region

In this section, the propagation area of the Tagus estuarine plume is identified, evaluating the role of the main forcings and how estuarine buoyancy affects the hydrography in different areas of the study region, by identifying regions where salinity increase or decrease.

In this section the calculated scenarios, ScD representative of the wind influence and ScE for discharge influence were used. In both scenarios, downwelling (16th November) and upwelling (18th November) favourable wind events were identified, and the mean salinity for each day calculated. The spatial salinity fields are obtained by subtracting ScB (coastal current + estuarine outflow) and ScC (coastal current + wind) to ScA (coastal current + estuarine outflow + wind) in order to obtain ScD (wind effect) and ScE (discharge effect). The river inflow for ScA and ScB is 3000 m^3s^{-1}.

The effect of southern/northern winds in the horizontal salinity structure is depicted in Figure 4.10. It can be observed a band of positive values of salinity close to the coast during downwelling (further south) and upwelling periods. This is induced by the wind stress that confines (expands) the plume close to the coast (to offshore) during downwelling (upwelling) periods. This is the result of the subtraction of the results of ScA and ScB, in which, this last scenario produces a low salinity band advected to the north with low

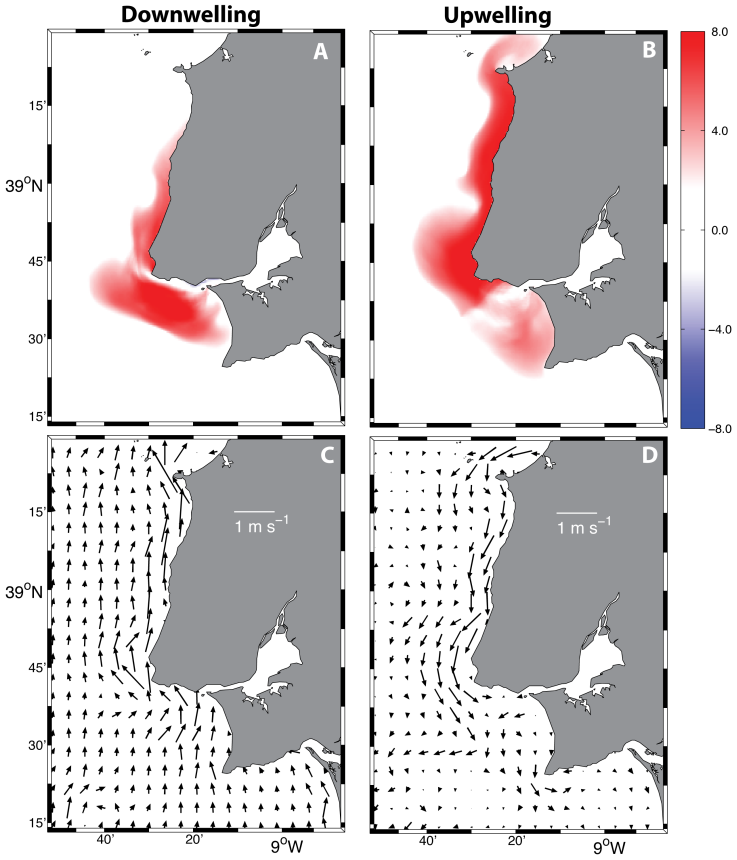

Figure 4.10: ScD results for a downwelling (A and C) and upwelling (B and D) events. A and B represent the salinity differences, while C and D mean surface current variation.

salinity values (estuarine).

It can be observed in the velocity fields that, surface currents are modulated by the wind, and that during downwelling (upwelling) the currents are to the north (south) in the region close to the west coast and near estuary mouth.

The effect of the estuarine discharge in the horizontal salinity structure is depicted in Figure 4.11 and is the result of the subtraction of ScA and ScC. In opposition to the results shown in Figure 4.10, here the effect of the estuarine discharge produces bands of negative values. That scenario of wind plus coastal current (ScC) presents higher values of salinity in the coastal region, which is expected since a null estuarine discharge was considered in this scenario. In the Figure 4.11 it is shown that, during downwelling events a band of negative values is found close to the estuary mouth and in the west coast. During upwelling events, the estuarine discharge is advected towards the south in the region of the Lisbon

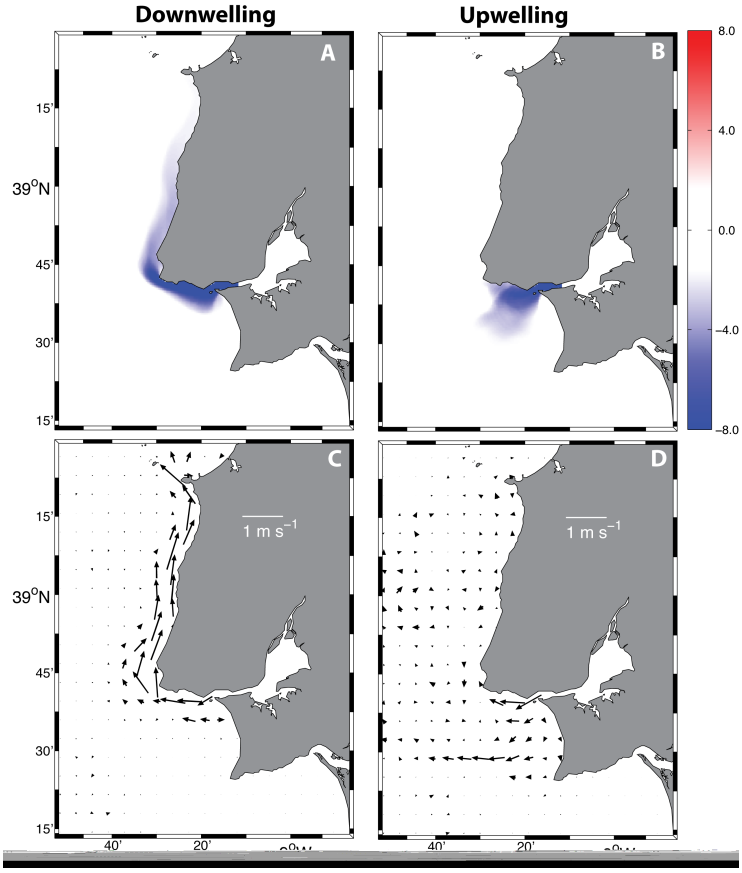

Figure 4.11: ScE results for a downwelling (A and C) and upwelling (B and D) events. A and B represent the salinity differences, while C and D mean surface current variation.

and no winds periods under different Tagus River discharges. Blue color represents a typical northward wind period, when the plume is confined close to the west coast in a direct response to wind forcing. Here, is observed a plume that goes from the Lisbon Bay until north of *Peniche* is observed. Orange color represents the observed SW path followed by the plume under southward winds, where it is advected onto the shelf as result of the combined effect of estuarine discharge and favourable upwelling winds. At last, the dashed grey lines represent the region of influence of the estuarine discharge under the no wind scenario. Here, the plume forms a bulge in the region close to the estuary mouth and due to the high estuarine discharge there is a band of estuarine water, which is advected up to the mouth until the regions close to *Peniche*.

4.2.3 Cross sections

The definition of surface-advected plume lies in the fact that the buoyant inflow remains primarily in shelf top, forming a thin layer that has little contact with the bottom, exceptionally near estuarine mouth (Yankovsky and Chapman, 1997). In this section, the x and y velocity components are evaluated through the cross-sections depicted in Figure 4.13. Here the main objective is to evaluate the plume thickness and preferential velocity directions, through, three cross-sections defined. Section S1, located at 38.67°N aims to represent the Tagus Estuary predominant outflow directions, therefore, u current

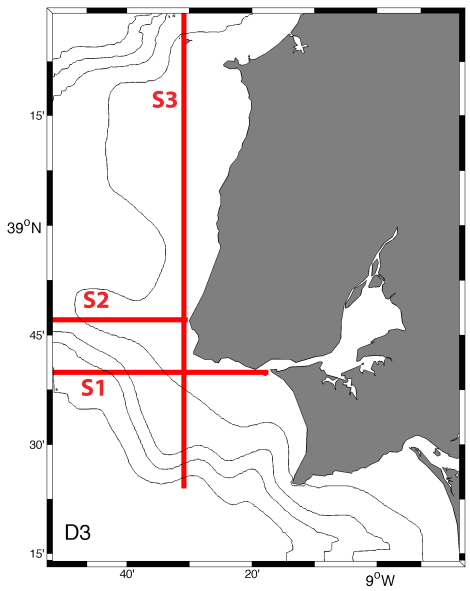

Figure 4.13: Cross-sections location in D3.

component was evaluated. In S2 cross-section the narrowest region of the D3, located at 38.79°N, v component is evaluated aiming to analyse the velocity component and plume path under northward winds. Finally, cross-sections S3 is a meridional slice at 9.52°W used to analyse the water movement due to a southern and northern wind pattern (u component is analysed). All the analysis in these sections were performed for ScA-A3, the scenario with full atmospheric forcing and the maximum river discharge value (5000 m^3s^{-1}).

For each section was chosen a downwelling (A), transitional (B) and upwelling (C) wind representative period. The results are depicted in Figures 4.14-4.16.

Under northward winds in S1 sections, the plume is observed between the 9.5°W and the coast. In the region adjacent to the coast (9.3°W) the plume comprises the full water column, while in the rest have a thickness of about 15 m (Figure 4.14 - A). The predicted currents show an intense negative u current component on the region where is observed the plume near the surface layers. Under the plume bulge is observed a positive u flow, that could be the reposition of the surface offshore advected waters, in order to maintain the equilibrium. A transition period in section S1 results in a lower thickness of the buoyant plume and its offshore displacement (Figure 4.14 - B). The thickness of the plume is reduced to 10 m, while in all the region located west of 9.5°W a negative u current velocity in the water column is observed, due to the water offshore advection. Finally, Figure 4.14 - C describes an upwelling event where the plume is confined to a region between 9.3°W

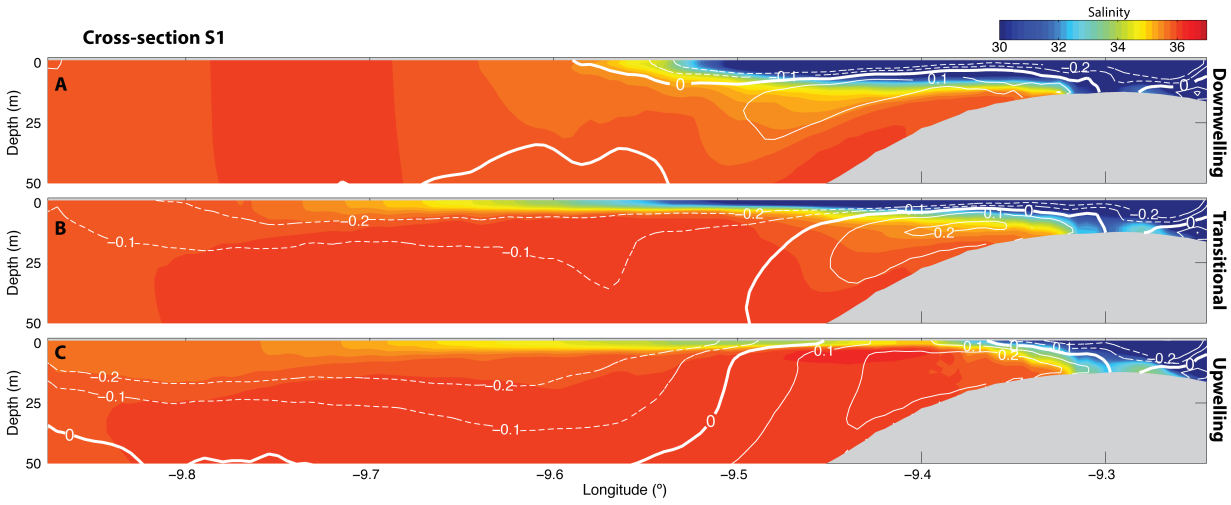

Figure 4.14: Salinity section S1. x component of velocity, with positive (solid lines) and negative (dashed lines) values. (A) downwelling, (B) transitional (C) and upwelling winds.

and the shore. The overall analysis of the S1 section reveal three different regions: near the estuary mouth mainly controlled by the estuarine discharge (9.3ºW - coast) with a negative u current component; a region between 9.5-9.3ºW with bottom positive u velocity component and an offshore region (west of 9.5ºW) that responds directly to wind.

In cross-sections S2, located in the region of *Cabo da Roca*, is possible to identify the estuarine buoyant flow in the first 10 m of the water column, in a narrow band of 12 km adjacent to coast during a downwelling event (Figure 4.15 - A). In this region, on the surface a strong northward flow induced by the plume is observed, while in depth a larger area with negative flow is observed. This could be due to a compensatory mechanism, observed by other authors under buoyant plumes (Mestres *et al.*, 2007; Jurisa and Chant, 2013). Offshore region of S2 (9.6ºW to west) shows positive v current components in all the column water, with higher values located in the middle section (near 9.7ºW) with values over 0.2 ms^{-1}.

In the transition between northward and southward winds, the plume spreads offshore for 18.5 km with a reduction of the plume thickness (Figure 4.15 - B). A detachment of the plume from the shore is noticeable. This could be the result of the negative v component high values. The offshore region presents a decrease of the positive v values in the superficial layers.

For southward winds the existent plume vanishes, while new buoyancy plumes are not

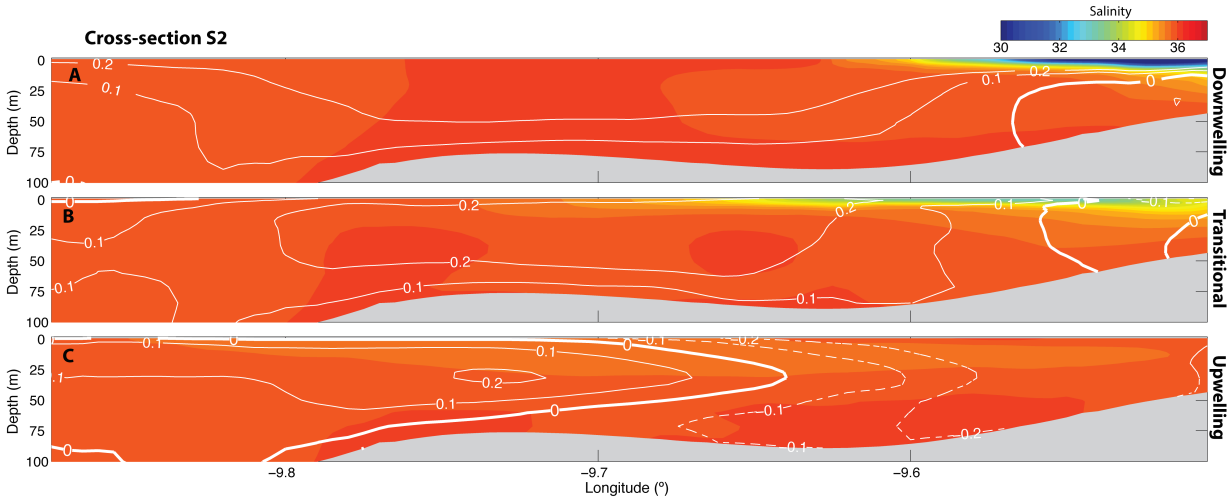

Figure 4.15: Salinity cross-section S2. y component of velocity, with positive (solid lines) and negative (dashed lines) values. Downwelling winds (A), transitional (B) and upwelling winds (C).

transported to this cross-shelf sections once that, under southward winds, the plume path is to SW (Figure 4.15 - C). Surface currents present a negative v component, while the vertical column present three distinct areas: near shelf with negative v component, an intermediate region (9.8-9.65ºW) with a positive intense v jet (near 30 m depth) compressed between negative v flows (top and bottom) and an offshore region with positive v component in most of the column.

Cross-sections S3 covers a wide region of the adjacent coast to Tagus Estuary. In this sections, under northward winds the plume can be identified in the region between 38.6-39.1ºN with a depth of about 15 m (Figure 4.16 - A). The south region of S3 presents negative u velocity values, while the northern region presents positive u velocity values. The central region have a complex pattern with the surface layer being forced by the buoyant plume.

With the wind rotation to south (upwelling favourable), surface currents begin to present negative u values (Figure 4.16 - B). The salinity field gradient decreases while is observed vertical mixing and an horizontal surface spreading. For the upwelling event, a plume break-up is observed and is possible to identify two distinct areas with low salinity (Figure 4.16 - C). The southern area is the offshore advection of the Tagus Estuary outflow, while the northern area is the result of the old plume field being advected from the coast

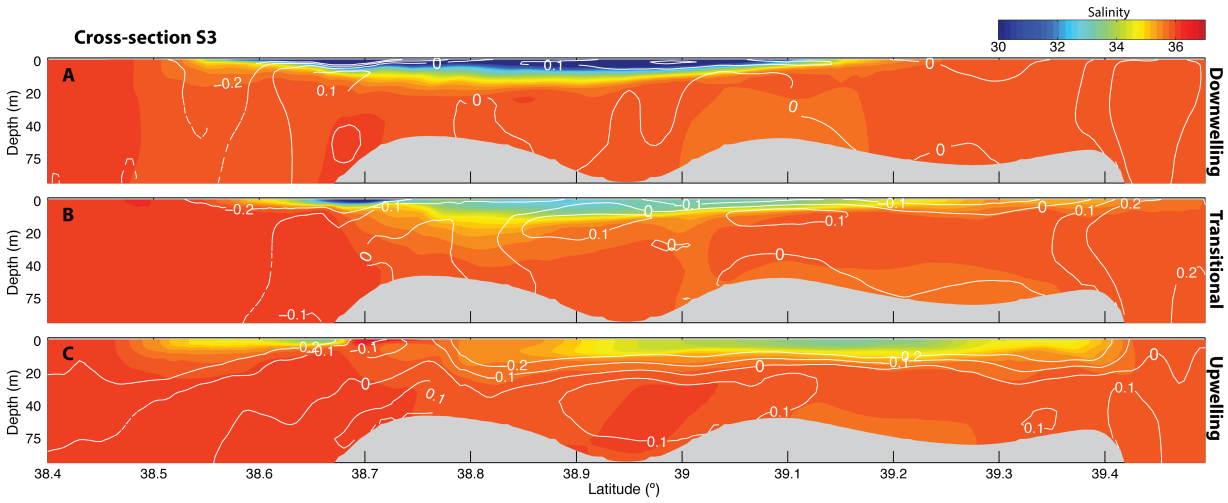

Figure 4.16: Salinity cross-section S3. x component of velocity, with positive (solid lines) and negative (dashed lines) values.(A) Downwelling winds, (B) transitional and (C) upwelling winds.

to offshore (crossing the section in analysis). Negative u velocity are observed for all the section. Nevertheless, bellow the 30 m is observed a positive u flow region, due to the upwelling of waters from the deeper areas.

North-south S3 cross-section analysis allowed to classify three distinct current zones (Figure 4.16): a southern region that presents negative u velocity values; a central region, between 38.6 and 39.4ºN, controlled by the wind and estuarine inflow; and the northern region where was observed positive u velocity. These results show a distinct hydrodynamic pattern between south and north regions of the domain, illustrating the region of influence of the Tagus estuarine plume.

An overall illustration of the typical observed plume pattern and v velocity component for the S2 cross-shelf section was performed and presented in Figure 4.17. The cross inside the circle represented positive v velocity and negative flows are represented by concentric circles; the dimension of the circles represents the magnitude of the signal. Under downwelling winds the presence of a plume confined to the shore is noticeable, with strong positive v

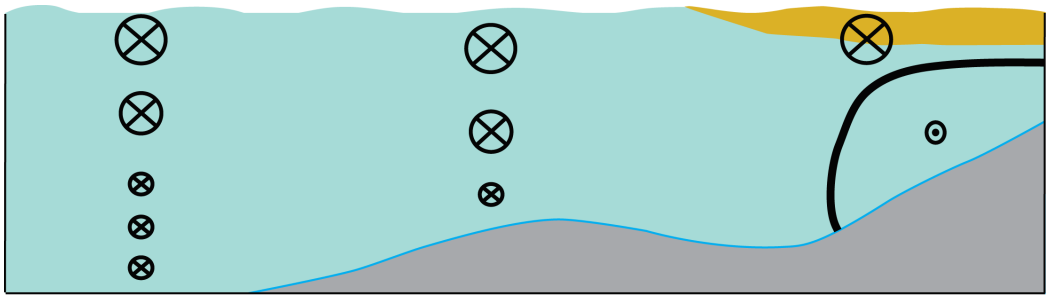

(a) Downwelling wind regime.

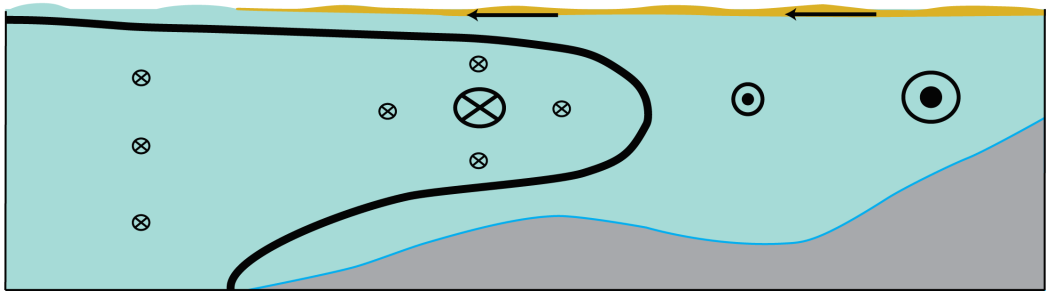

(b) Upwelling wind regime.

Figure 4.17: Illustration of y velocity components in a cross-section north of *Cabo da Roca* for river discharger higher than 1500 m^3s^{-1} for (a) downwelling and (b) upwelling events. Black line represent the 0 ms^{-1} velocity component and black vectors represent a west transport.

values and, underneath a weak negative v value, while in offshore region presents higher positive values in the upper layers (Figure 4.17a).

For an upwelling event, the offshore spreading of the plume (to the west)is observed, while the plume shrunk (Figure 4.17b). Positive v velocities were observed in the near shelf, in the bottom and top layers, though is observed a relative strong negative v jet in the middle of the water column.

Chapter 5

Conclusion

All the proposed objectives for this study were achieved, within the main goal to research the Tagus Estuarine plume under different wind regimes and river discharges. With that purpose, a new circulation and transport model (MOHID) application was implemented.

An offline 2D circulation and transport model was implemented for the Tagus Estuary. This implementation was previously validated by Vaz *et al.* (2011) and Silva (2012) and used to calculate the exchange flow between the estuary and the near shelf region, to be used as landward boundary condition in the coastal model.

The costal application is a 3D baroclinic model based on PCOMS model, with a spatial horizontal resolution of 0.06º and 50 vertical layers. A downscaling methodology was used to improve spatial resolution to 500 m in the Tagus ROFI. The model validation was successfully performed comparing predictions with avilable data sets.

The coastal model predictions of surface currents were validated trough the comparison with a Portuguese Navy HF radar dataset. The results show a good reproduction of the observations with a mean RMSE of local amplitude of 22.0% and 17.8% for u and v velocity components, respectively, with the same accuracy degree of other identical studies. The coastal model transport validation (water temperature and salinity) was performed by comparing model results and remote sensing imagery from MODIS sensor. Results shown that model SST show an identical surface pattern, with a maximum deviation lower than 2 ºC. For surface salinity field assessment, MODIS nLw555 turbidity band was used to identify the plume bulge at the Lisbon Bay. Results showed that the model predictions of the plume dimension and location were identical to remote sensing high turbidity regions at the region.

The coupling methodology was then considered able to reproduce observations and,

therefore able to simulate estuarine and coastal processes for the study region.

After the model validation, five scenarios were implemented to study the plume under different wind and discharge events. Scenario A was considered as the reference scenario, with a complete atmosphere and river discharge forcing; scenario B is a no wind stress scenario and scenario C does not consider estuarine discharges. Scenarios D and E resulted from the subtraction of scenario A - scenario B and scenario A - scenario C, respectively. For each scenario, three distinct simulations were performed using different river discharges (1500, 3000 and 5000 m^3s^{-1}).

The use of self-organizing maps, an unsupervised neural networks, allowed to identify the variability of the region. That methodology was used to assess the scenarios A, B and C. Results showed that the salinity pattern was controlled by the discharge during high river discharge, while for low discharge values the wind stress was the main forcing. In absence of estuarine discharge, surface salinity has no relation with wind, and the coastal circulation was the predominant forcing.

The differences obtained in the scenarios D and E results give a spatial idea about regions of influence of discharge and wind, respectively. This study allowed to identify the influence area of the wind and discharges in the plume propagation. The results show that the river discharge has a direct role on the plume dimension, with higher discharge values producing larger bulges. Surface currents were also analysed and the results show that the estuarine discharges produce an increase of current velocity, under downwelling winds, near 0.9 ms^{-1} for a 3000 m^3s^{-1} river discharge, while for upwelling winds, an increase of 0.2 ms^{-1} was observed.

The plume path under downwelling favourable winds follows a northward direction, following the coastline, while for upwelling favourable winds, the observed flow directions is the SW. This represents a confinement and expansion of the Tagus estuarine plume to and from the coast. In the absence of wind stress, the estuarine jet is controlled by the Coriolis force with a rotation to the right of the flow and the plume propagation to the north. For all the analysed wind regimes, the buoyant plume dimensions were controlled by the river discharge.

In order to evaluate the plume thickness, three cross-sections for salinity along the D3 domain were set. At same time, the horizontal velocity components were analysed. Results shown that with a river discharge of 5000 m^3s^{-1}, the estuary mouth region is fully dominated by estuarine waters in all wind regimes. The higher plume thickness was registered under downwelling events, 15 m depth, being reduced with the wind rotation to

south (10 m). Horizontal currents show the quick response of the circulation to the wind rotation, specially in the region near shore. Under the plume bulge a persistent jet was observed, with opposite direction to the plume propagation.

In overall, under downwelling events the plume is advected to the north, reaching, as far as, *Peniche* for a river discharge of 5000 m^3s^{-1}, while for a river discharge of 1500 m^3s^{-1} its excursion is limited to *Cabo da Roca*. Upwelling events shown a SW plume advection confined to the Lisbon Bay for all the studied river discharge.

Estuarine plumes are relevant to many coastal environments aspects, such as: biological production enhancement, primary production improving, costal pollution and geochemical transport. Many of those factors have strong impact and are socio-economic important to the region population. As future work, the incorporation of a biogeochemical model is proposed. Recent news indicate that the Barreiro Harbour will be upgraded to an important harbour, expecting an increase of maritime traffic. That possibility, increases the importance of the study of oil spills, being that a possible new module incorporation to the model. An increase of the atmospheric model horizontal resolution could improve the circulation predictions, especial in the mouth region of the estuary. The online coupling of the estuarine and coastal application in a unique one, is also one of the future objectives.

Bibliography

Alcoforado, M. J. (1987). Brisas Estivais Do Tejo E Do Oceano Na Região De Lisboa. *Finisterrra*, 22(43):71–112.

Alcoforado, M. J. and Lopes, A. (2003). Windfields and temperature patterns in Lisbon (Portugal) and their modification due to city growth. In *5th International Conference on Urban Climate (ICUC5)*, 4 p., Lodz.

Ambar, I. and Fiúza, A. (1994). Some features of the Portugal Current System: A poleward slope undercurrent, an upwelling-related summer southward flow and an autumn-winter poleward coastal surface current. *Second International Conference on Air-Sea Interaction and on Meteorology and Oceanography of the Coastal Zone*, Proceeding:286–287.

Angi (2011). *West Coast Of Europe And Northwest Africa - Sailing Directions (Enroute)*, 143. Hydrographic/Topographic Center, Washington, D.C., thirteenth edição.

Arakawa, A. (1966). Computational Design for Long-Term Numerical Integration of the Equations of Fluid Motion: Two-Dimensional Incompressible Flow. Part I. *Journal of Computational Physics*, 1(1):119–143, doi:10.1006/jcph.1997.5697.

Boicourt, W. C. *The circulation of water on the continental shelf from Chesapeake Bay to Cape Hatteras*. PhD thesis, Johns Hopkins University, (1973), 183 p.

Chao, S. (1988). Wind-Driven Motion of Estuarine Plumes. *Journal of Physical Oceanography*, 18(8):1144–1166, doi:10.1175/1520-0485(1988)018<1144:WDMOEP>2.0.CO;2.

Chao, S. and Boicourt, W. C. (1986). Onset of Estuarine Plumes. *Journal of Physical Oceanography*, 16:2137–2149, doi:10.1175/1520-0485(1986)016<2137:OOEP>2.0.CO;2.

Chapman, R., Shay, L., Graber, H., Edson, J., Karachintsev, A., Trump, C., and Ross, D. (1997). On the accuracy of HF radar surface current measurements: Intercom-

parisons with ship-based sensors. *Journal of Geophysical Research*, 102(C8):18737, doi:10.1029/97JC00049.

Chapra, S. (1997). *Surface Water-Quality Modeling*. McGraw-Hill, New York.

Cheng, P. and Wilson, R. E. (2006). Temporal variability of vertical nontidal circulation pattern in a partially mixed estuary: Comparison of self-organizing map and empirical orthogonal functions. *Journal of Geophysical Research*, 111(C12):C12021, doi:10.1029/2005JC003241.

Coelho, H., Neves, R., and Leitão, P. C. (2000). A Numerical Model of the Guadiana Estuary. In *3rd Symposium on the Iberian Atlantic Margin*, 1.

Dagg, M., Benner, R., Lohrenz, S., and Lawrence, D. (2004). Transformation of dissolved and particulate materials on continental shelves influenced by large rivers: plume processes. *Continental Shelf Research*, 24(7-8):833–858, doi:Doi 10.1016/J.Csr.2004.02.003.

Defant, A. (1960). *Physical oceanography - Vol. II*. Pergamon Press, Oxford, 598 p.

Dias, J. M. *Comparação dos resultados de um modelo numérico bi-dimensional com observacções de corrente no estuário do Tejo*. PhD thesis, University of Lisbon, Portugal, (1993), 244 p.

Dias, J. M. and Lopes, J. (2006). Implementation and assessment of hydrodynamic, salt and heat transport models: The case of Ria de Aveiro Lagoon (Portugal). *Environmental Modelling & Software*, 21(1):1–15, doi:10.1016/j.envsoft.2004.09.002.

Dias, J. M., Sousa, M. C., Bertin, X., Fortunato, A. B., and Oliveira, A. (2009). Numerical modeling of the impact of the Ancão Inlet relocation (Ria Formosa, Portugal). *Environmental Modelling and Software*, 24(6):711–725.

Dias, J. M., Valentim, J. M., and Sousa, M. C. (2013). A numerical study of local variations in tidal regime of Tagus estuary, Portugal. *PLoS ONE*, 8, doi:10.1371/journal.pone.0080450.

Fernandes, C. and Agostinho, P. (2008). The Sines HF Radar Experience: Analysis of the results. In *9th. Littoral Conference*, Venice.

Fernandes, R. *Modelação Operacional no Estuário do Tejo*. PhD thesis, Instituto Superior Técnico, (2005), 106 p.

Fernández-Nóvoa, D., Mendes, R., DeCastro, M., Dias, J., Sánchez-Arcilla, A., and Gómez-Gesteira, M. (2015). Analysis of the influence of river discharge and wind on the Ebro turbid plume using MODIS-Aqua and MODIS-Terra data. *Journal of Marine Systems*, 142:40–46, doi:10.1016/j.jmarsys.2014.09.009.

Fiúza, A., Macedo, M., and Guerreiro, M. (1982). Climatological Space and Time Variation of the Portuguese Coastal Upwelling. *Oceanologia Acta*, 5(1):31–40.

Fofonoff, P. and Millard, R. (1983). Algorithms for computation of fundamental properties of seawater. *Unesco Tech*, 44:Eqn.(31) p.39.

Fong, D. A. and Geyer, W. R. (2001). Response of a river plume during an upwelling favorable wind event. *Journal of Geophysical Research*, 106(C1):1067, doi:10.1029/2000JC900134.

Fong, D. A. and Geyer, W. R. (2002). The Alongshore Transport of Freshwater in a Surface-Trapped River Plume. *Journal of Physical Oceanography*, 32(3):957–972, doi:10.1175/1520-0485(2002)032<0957:TATOFI>2.0.CO;2.

Fortunato, A., Baptista, A. M., and Luettich, R. A. (1997). A three-dimensional model of tidal currents in the mouth of the Tagus estuary. *Continental Shelf Research*, 17(14):1689–1714, doi:10.1016/S0278-4343(97)00047-2.

Fortunato, A., Oliveira, A., and Baptista, A. M. (1999). On the effect of tidal flats on the hydrodynamics of the Tagus estuary. *Oceanologica Acta*, 22(1):31–44, doi:10.1016/S0399-1784(99)80030-9.

Franz, G., Pinto, L., Ascione, I., Mateus, M., Fernandes, R., Leitão, P. C., and Neves, R. (2014). Modelling of cohesive sediment dynamics in tidal estuarine systems: Case study of Tagus estuary, Portugal. *Estuarine, Coastal and Shelf Science*, 151:34–44, doi:10.1016/j.ecss.2014.09.017.

Frouin, R., Fiúza, A. F. G., Ambar, I., and Boyd, T. J. (1990). Observations of a poleward surface current off the coasts of Portugal and Spain during winter. *Journal of Geophysical Research*, 95(C1):679, doi:10.1029/JC095iC01p00679.

Garvine, R. W. (1974). Physical features of the Connecticut River outflow during high discharge. *Journal of Geophysical Research*, 79:831, doi:10.1029/JC079i006p00831.

Garvine, R. W. (1982). A steady state model for buoyant surface plume hydrodynamics in coastal waters. *Tellus A*, pp: 293–306, doi:10.3402/tellusa.v34i3.10813.

Gomez-Gesteira, M., Montero, P., Prego, R., Taboada, J. J., Leitao, P., Ruiz-Villarreal, M., Neves, R., and Perez-Villar, V. (1999). A two-dimensional particle tracking model for pollution dispersion in A Coruna and Vigo Rias (NW Spain). *Oceanologica Acta*, 22(2):167–177, doi:10.1016/S0399-1784(99)80043-7.

Hetland, R. D. (2005). Relating River Plume Structure to Vertical Mixing. *Journal of Physical Oceanography*, 35(9):1667–1688, doi:10.1175/JPO2774.1.

Hewitson, B. C. and Crane, R. G. (2002). Self-organizing maps: Applications to synoptic climatology. *Climate Research*, 22:13–26, doi:10.3354/cr022013.

Hickey, B. M., Pietrafesa, L. J., Jay, D. A., and Boicourt, W. C. (1998). The Columbia River Plume Study: Subtidal variability in the velocity and salinity fields. *Journal of Geophysical Research*, 103:10339, doi:10.1029/97JC03290.

Horner-Devine, A. R., Jay, D. A., Orton, P. M., and Spahn, E. Y. (2009). A conceptual model of the strongly tidal Columbia River plume. *Journal of Marine Systems*, 78:460–475, doi:10.1016/j.jmarsys.2008.11.025.

Jurisa, J. T. and Chant, R. J. (2013). Impact of Offshore Winds on a Buoyant River Plume System. *Journal of Physical Oceanography*, 43(12):2571–2587, doi:10.1175/JPO-D-12-0118.1.

Kohonen, T. (1982). Self-organized formation of topologically correct feature maps. *Biological Cybernetics*, 43(1):59–69, doi:10.1007/BF00337288.

Kohonen, T. (1988). The 'neural' phonetic typewriter. *Computer*, 21(3):11–22, doi:10.1109/2.28.

Kourafalou, V. H., Oey, L.-Y., Wang, J. D., and Lee, T. N. (1996). The fate of river discharge on the continental shelf: 1. Modeling the river plume and the inner shelf coastal current. *Journal of Geophysical Research*, 101(C2):3415, doi:10.1029/95JC03024.

Kropp, J. and Klenke, T. (1997). Phenomenological pattern recognition in the dynamical structures of tidal sediments from the German Wadden Sea. *Ecological Modelling*, 103(2-3):151–170, doi:10.1016/S0304-3800(97)00083-5.

Legates, D. R. and McCabe, G. J. (1999). Evaluating the use of 'goodness-of-fit' measures in hydrologic and hydroclimatic model validation. *Water Resources Research*, 35(1):233–241, doi:10.1029/1998WR900018.

Leitão, P., Coelho, H., Santos, A., and Neves, R. (2005). Modelling the main features of the Algarve coastal circulation during July 2004: A downscaling approach. *Journal of Atmospheric & Ocean Science*, 10(4):421–462, doi:10.1080/17417530601127704.

Leitão, P. C. *Modelo de Dispersao Lagrangeano Tridimensional*. PhD thesis, Technical University of Lisbon, (1996).

Leitão, P. C. *Integracao de Escalas e Processos na Modelacao do Ambiente Marinho*. PhD thesis, Universidade Técnica de Lisboa, (2003).

Leitão, P. C., Neves, R., Coelho, H., Braunschweig, F., Leitão, J., and Margin, A. (2000). 3D Hydrodynamic Modelling of the Tagus Region of Fresh Water Influence. *Stress: The International Journal on the Biology of Stress*, pp: 3–5.

Liu, Y., MacCready, P., and Hickey, B. M. (2009). Columbia River plume patterns in summer 2004 as revealed by a hindcast coastal ocean circulation model. *Geophysical Research Letters*, 36(2):n/a–n/a, doi:10.1029/2008GL036447.

Liu, Y. and Weisberg, R. H. (2005). Patterns of ocean current variability on the West Florida Shelf using the self-organizing map. *Journal of Geophysical Research*, 110(C6):C06003, doi:10.1029/2004JC002786.

Liu, Y. and Weisberg, R. H. (2007). Ocean Currents and Sea Surface Heights Estimated across the West Florida Shelf. *Journal of Physical Oceanography*, 37(6):1697–1713, doi:10.1175/JPO3083.1.

Liu, Y., Weisberg, R. H., and He, R. (2006a). Sea surface temperature patterns on the West Florida Shelf using growing hierarchical self-organizing maps. *Journal of Atmospheric and Oceanic Technology*, 23(2):325–338, doi:10.1175/JTECH1848.1.

Liu, Y., Weisberg, R. H., and Mooers, C. N. K. (2006b). Performance evaluation of the self-organizing map for feature extraction. *Journal of Geophysical Research*, 111(C5):C05018, doi:10.1029/2005JC003117.

Liu, Y., Weisberg, R. H., and Shay, L. K. (2007). Current Patterns on the West Florida Shelf from Joint Self-Organizing Map Analyses of HF Radar and ADCP Data. *Journal of Atmospheric and Oceanic Technology*, 24(4):702–712, doi:10.1175/JTECH1999.1.

Lobo, V. (2009). Application of self-organizing maps to the maritime environment. In *Lecture Notes in Geoinformation and Cartography*, pp: 19–36.

Lopes, A., Alves, E., Alcoforado, M. J., and Machete, R. (2013). Lisbon Urban Heat Island Updated: New Highlights about the Relationships between Thermal Patterns and Wind Regimes. *Advances in Meteorology*, 2013:1–11, doi:10.1155/2013/487695.

Loureiro, J. (1979). *Curvas de Duração dos Caudais Médios Diários no Rio Tejo.* Relatório técnico, Direcção Geral de Recursos e Aproveitamentos Hidráulicos, Lisboa.

Lyard, F., Lefevre, F., Letellier, T., and Francis, O. (2006). Modelling the global ocean tides: modern insights from FES2004. *Ocean Dynamics*, 56(5-6):394–415, doi:Doi 10.1007/S10236-006-0086-X.

Macedo, M. E. (2006). *Caracterização de Caudais – Rio Tejo Ano Hidrologico de 2005/06.* Relatório técnico, Direcção de Serviços de Monitorização Ambiental, Lisboa.

Maillard, C. (1986). *Atlas hydrologique de l'Atlantique nord-est.* IFREMER, Brest, 133 p.

Malhadas, M. S., Leitão, P. C., Silva, A., and Neves, R. (2009). Effect of coastal waves on sea level in Óbidos Lagoon, Portugal. *Continental Shelf Reaserch*, 29(9):1240–1250, doi:10.1016/j.csr.2009.02.007.

Martins, F., Leitão, P. C., Silva, A., and Neves, R. (2001). 3D modelling in the Sado estuary using a new generic vertical discretization approach. *Oceanologica Acta*, 24:51–62, doi:10.1016/S0399-1784(01)00092-5.

Martins, F., Neves, R., and Leitão, P. C. (1998). A three-dimensional hydrodynamic model with generic vertical coordinate. In *Hydro-informatics*, number 98, pp: 1403–1410.

Mason, E., Coombs, S., and Oliveira, P. B. (2005). *An overview of the literature concerning the oceanography of the eastern North Atlantic region.* Relatório técnico, IPIMAR - Série digital, Lisboa, 58 p.

Mateus, M., Riflet, G., Chambel, P., Fernandes, L., Fernandes, R., Juliano, M., Campuzano, F., De Pablo, H., and Neves, R. (2012). An operational model for the West Iberian coast: Products and services. *Ocean Science*, 8(4):713–732, doi:10.5194/os-8-713-2012.

Mendes, R. *Modelação numérica da pluma estuarina da Ria de Aveiro: estudo preliminar.* Msc thesis, Universidade de Aveiro, (2010), 50 p.

Mendes, R., Vaz, N., Fernández-Nóvoa, D., da Silva, J., DeCastro, M., Gómez-Gesteira, M., and Dias, J. (2014). Observation of a turbid plume using MODIS imagery: The

case of Douro estuary (Portugal). *Remote Sensing of Environment*, 154:127–138, doi:10.1016/j.rse.2014.08.003.

Mestres, M., Sierra, J. P., and Sánchez-Arcilla, a. (2007). Factors influencing the spreading of a low-discharge river plume. *Continental Shelf Research*, 27(16):2116–2134, doi:10.1016/j.csr.2007.05.008.

Miranda, R. *Nitrogen Biogeochemical Cycle Modeling in the North Atlantic Ocean*. PhD thesis, Technical University of Lisbon, (1997).

NASA, O. B. (2015). SST Quality Flags. Availabel in: `http://oceancolor.gsfc.nasa.gov/cms/atbd/sst/doc/html/flag.html` [Consulted in 2015-07-10].

NCEP (2003). *The GFS Atmospheric Model - NCEP Office Note 442. Global Climate and Weather Modeling Branch, EMC, Camp Springs, Maryland*. Relatório técnico November, Global Climate and Weather Modeling Branch, EMC, Camp Springs, Maryland, 14 p.

Neves, F. *Dynamics and hydrology of the Tagus estuary : results from in situ observations*. Phd thesis, University of Lisbon, (2010), 210 p.

Neves, R. *Étude Experimentale et Modélisation des Circulations Trasitoire et Résiduelle dans l'Estuaire du Sado*. PhD thesis, Univ. Liège, (1985).

Nezlin, N. P. and DiGiacomo, P. M. (2005). Satellite ocean color observations of stormwater runoff plumes along the San Pedro Shelf (southern California) during 1997–2003. *Continental Shelf Research*, 25(14):1692–1711, doi:10.1016/j.csr.2005.05.001.

Nishihama, M., Wolfe, R., and Solomon, D. (1997). *MODIS Level 1A Earth Location: Algorithm Theoretical Basis Document - Version 3.0*. Relatório técnico, NASA/Goddard Spaceflight Center, 147 p.

Oliveira, A., Fortunato, A., and Rego, J. a. (2006). Effect of morphological changes on the hydrodynamics and flushing properties of the Óbidos lagoon (Portugal). *Continental Shelf Research*, 26:917–942, doi:10.1016/j.csr.2006.02.011.

Oliveira, P. B., Nolasco, R., Dubert, J., Moita, T., and Peliz, A. (2009). Surface temperature, chlorophyll and advection patterns during a summer upwelling event off central Portugal. *Continental Shelf Research*, 29(5-6):759–774, doi:10.1016/j.csr.2008.08.004.

Otero, P., Ruiz-Villarreal, M., and Peliz, A. (2008). Variability of river plumes off Northwest Iberia in response to wind events. *Journal of Marine Systems*, 72(1-4):238–255, doi:10.1016/j.jmarsys.2007.05.016.

O'Donncha, F., Hartnett, M., Nash, S., Ren, L., and Ragnoli, E. (2015). Characterizing observed circulation patterns within a bay using HF radar and numerical model simulations. *Journal of Marine Systems*, 142:96–110, doi:10.1016/j.jmarsys.2014.10.004.

Pawlowicz, R., Beardsley, B., and Lentz, S. (2002). Classical Tidal Harmonic Analysis Including Error Estimates in MATLAB using T_TIDE. *Computers and Geosciences*, 28:929–937.

Pereira, S. C., Carvalho, C., Ferreira, J., Nunes, J. P., Keizer, J. J., and Rocha, A. (2013). Simulation of a persistent medium-term precipitation event over the western Iberian Peninsula. *Hydrology and Earth System Sciences*, 17(10):3741–3758, doi:10.5194/hess-17-3741-2013.

Pérez, F. F., Castro, C. G., Álvarez Salgado, X. a., and Ríos, A. F. (2001). Coupling between the Iberian basin - Scale circulation and the Portugal boundary current system: A chemical study. *Deep-Sea Research Part I: Oceanographic Research Papers*, 48(6):1519–1533, doi:10.1016/S0967-0637(00)00101-1.

Petrou, M. (2004). Preface. *Pattern Recognition Letters*, 25(13):1459, doi:10.1016/j.patrec.2004.05.021.

Picado, A., Lopes, C., Mendes, R., Vaz, N., and Dias, J. M. (2013). Storm surge impact in the hydrodynamics of a tidal lagoon: the case of Ria de Aveiro. *Journal of Coastal Research*, SI65(SI65):796–801, doi:10.2112.

Portela, L. *Mathematical modelling of hydrodynamic and water quality processes in the Tagus estuary*. PhD thesis, Universidade Tecnica de Lisboa, (1996), 240 p.

Reusch, D. B., Hewitson, B. C., and Alley, R. B. (2005). Towards ice-core-based synoptic reconstructions of West Antarctic climate with artificial neural networks. *International Journal of Climatology*, 25:581–610, doi:10.1002/joc.1143.

Richardson, A., Risien, C., and Shillington, F. (2003). Using self-organizing maps to identify patterns in satellite imagery. *Progress in Oceanography*, 59(2-3):223–239, doi:10.1016/j.pocean.2003.07.006.

Riflet, G. *Downscaling large-scale Ocean basin solutions in regional three-dimensional hydrodynamic models*. Phd thesis, Technical University of Lisbon, (2010), 273 p.

Ríos, A. F., Pérez, F. F., and Fraga, F. (1992). Water masses in the upper and middle North Atlantic Ocean east of the Azores. *Deep Sea Research Part A. Oceanographic Research Papers*, 39(3-4):645–658, doi:10.1016/0198-0149(92)90093-9.

Risien, C. M. (2004). Variability in satellite winds over the Benguela upwelling system during 1999–2000. *Journal of Geophysical Research*, 109(C3):C03010, doi:10.1029/2003JC001880.

Rodrigues, J. G., Mendes, R., and Dias, J. M. (2012). Alterações Hidrodinâmicas no Estuário do Rio Lima: Resposta à sua Evolução Morfológica. In *V Congresso Brasileiro de Oceanografia*, Rio de Janeiro, Brasil.

Rodrigues, J. G., Mendes, R., Pereira, S. C., Vaz, N., and Dias, J. M. (2015). Hidrologia da Zona Costeira Adjacente ao Estuário Do Tejo. In *9ª Simpósio de Meteorologia e Geofísica da Associação Portuguesa de Meteorologia e Geofísica*, 6 p., Tavira.

Rusu, L., Bernardino, M., and Soares, C. G. (2009). Influence of Wind Resolution on the Prediction of Waves Generated in an Estuary. *Journal of Coastal Research*, SI 56:1419–1423.

Santos, A. J. *Modelo Hidrodinâmico Tridimensional de Circulação Oceânica e Estuarina*. PhD thesis, Universidade Técnica de Lisboa, (1995).

Saraiva, S., Pina, P., Martins, F., Santos, M., Braunschweig, F., and Neves, R. (2007). Modelling the influence of nutrient loads on Portuguese estuaries. *Hydrobiologia*, 587(1):5–18.

Schuenemann, K. C. and Cassano, J. J. (2010). Changes in synoptic weather patterns and Greenland precipitation in the 20th and 21st centuries: 2. Analysis of 21st century atmospheric changes using self-organizing maps. *Journal of Geophysical Research: Atmospheres*, 115, doi:10.1029/2009JD011706.

Sentchev, A., Forget, P., Barbin, Y., and Yaremchuk, M. (2013). Surface circulation in the Iroise Sea (W. Brittany) from high resolution HF radar mapping. *Journal of Marine Systems*, 109-110(SUPPL.), doi:10.1016/j.jmarsys.2011.11.024.

Silva, A. *Coccolithophores in coastal waters: Lisbon Bay, Portugal*. Phd thesis, Universidade de Lisboa, (2008), 211 p.

Silva, A. J. R., Leitão, P. C., Leitão, J., Braunschweig, F., and Neves, R. (2002). Ria Formosa 3D Hydrodynamic Model . A Contribution for the Understanding of the Faro-Olhão Inlet Processes. In *Litoral 2002, The Changing Coast, EUROCOAST/EUCC*, pp: 197–207.

Silva, J. M. *Hydrodynamic effects in Ria de Aveiro and Tagus estuary salt marshes*. Msc thesis, Universidade de Aveiro, (2012).

Skamarock, W. C., Klemp, J. B., Dudhia, J. B., Gill, D. O., Barker, D. M., Duda, M. G., Huang, X. Y., Wang, W., and Powers, J. G. (2008). *A description of the Advanced Research WRF Version 3, NCAR Technical Note TN-475+STR*. Relatório técnico, National Center for Atmospheric Research, Boulder, Colorado, 113 p.

Sousa, M. C. *Modelling the Minho river plume intrusion into the rias baixas*. Phd thesis, Universidade de Aveiro, (2013), 136 p.

Sousa, M. C., Vaz, N., Alvarez, I., and Dias, J. M. (2013). Effect of Minho estuarine plume on Rias Baixas: numerical modeling approach. *Journal of Coastal Research*, (Special Issue No. 65):2059–2064, doi:10.2112/SI65-348.1.

Sousa, M. C., Vaz, N., Alvarez, I., Gomez-Gesteira, M., and Dias, J. M. (2014a). Influence of the minho river plume on the rias baixas (nw of the iberian peninsula). *Journal of Marine Systems*, 139:248–260, doi:10.1016/j.jmarsys.2014.06.012.

Sousa, M. C., Vaz, N., Alvarez, I., Gomez-Gesteira, M., and Dias, J. M. (2014b). Modeling the Minho River plume intrusion into the Rias Baixas (NW Iberian Peninsula). *Continental Shelf Research*, 85:30–41, doi:10.1016/j.csr.2014.06.004.

Sousa, T. *Previsão Meteorológica em Portugal Continental utilizando o modelo operacional e de investigação MM5*. Msc thesis, Universidade Técnica de Lisboa, (2002), 150 p.

Stefnsson, U. and Richards, F. A. (1963). Processes contributing to the nutrient distributions off the Columbia River and Strait of Juan de Fuca. *Limnology and Oceanography*, 8:394–410, doi:10.4319/lo.1963.8.4.0394.

Stewart, R. H. and Joy, J. W. (1974). HF radio measurements of surface currents. *Deep Sea Research and Oceanographic Abstracts*, 21(12):1039–1049, doi:10.1016/0011-7471(74)90066-7.

Takano, K. (1954a). On the salinity and the velocity distributions off the mouth of a river. *Journal of the Oceanographical Society of Japan*, 10(3):92–98.

Takano, K. (1954b). On the velocity distribution off the mouth of a river. *J. Oceanogr. Soc. Japan*, 10:60–64.

Takano, K. (1955). A complementary note on the diffusion of the seaward river flow off the mouth. *Journal of the Oceanographical Society of Japan*, 11(4):147–149.

Trancoso, A. R. R. *Operational Modelling as a Tool in Wind Power Forecasts and Meteorological Warnings*. Phd thesis, Universidade Técnica de Lisboa, (2012), 120 p.

Trujillo, D., Kelly, F., Perez, J., Riddles, H., and Bonner, J. (2004). Accuracy of surface current velocity measurements obtained from HF radar in Corpus Christi Bay, Texas. In *IEEE International Geoscience and Remote Sensing Symposium*, 2, pp: 1179–1182. IEEE.

Vale, C. and Sundby, B. r. (1987). Suspended sediment fluctuations in the Tagus estuary on semi-diurnal and fortnightly time scales. *Estuarine, Coastal and Shelf Science*, 25(5):495–508, doi:10.1016/0272-7714(87)90110-7.

Valente, A. S. and da Silva, J. C. B. . (2009). On the observability of the fortnightly cycle of the Tagus estuary turbid plume using MODIS ocean colour images. *Journal of Marine Systems*, 75(1-2):131–137, doi:10.1016/j.jmarsys.2008.08.008.

Vaz, N. *Estudo dos processos de transporte de calor e de sal no Canal do Espinheiro (Ria de Aveiro)*. Phd thesis, Universidade de Aveiro, (2007), 151 p.

Vaz, N. and Dias, J. M. (2014). Residual currents and transport pathways in the Tagus estuary, Portugal : the role of freshwater discharge and wind. *Journal of Coastal Research*, 70(SI):610–616, doi:10.2112/SI70-103.1.

Vaz, N., Dias, J. M., and Leitão, P. C. (2009a). Three-dimensional modelling of a tidal channel: The Espinheiro Channel (Portugal). *Continental Shelf Research*, 29(1):29–41, doi:10.1016/j.csr.2007.12.005.

Vaz, N., Dias, J. M., Leitão, P. C., and Nolasco, R. (2007). Application of the Mohid-2D model to a mesotidal temperate coastal lagoon. *Computers & Geosciences*, 33(9):1204–1209, doi:10.1016/j.cageo.2007.02.001.

Vaz, N., Fernandes, L., Leitão, P. C., Dias, J. M., and Neves, R. (2009b). The Tagus Estuarine Plume Induced By Wind and River Runoff: Winter 2007 Case Study. *Journal of Coastal Research*, IS(56):1090–1094.

Vaz, N., Mateus, M., Plecha, S., Sousa, M. C., Leitão, P. C., Neves, R., and Dias, J. M. (2015). Modeling SST and chlorophyll patterns in a coupled estuary-coastal system of Portugal: The Tagus case study. *Journal of Marine Systems*, 147:123–137, doi:10.1016/j.jmarsys.2014.05.022.

Vaz, N., Mateus, N., and Dias, J. M. (2011). Semidiurnal and spring-neap variations in the Tagus Estuary: Application of a process-oriented hydro-biogeochemical model. *Journal of Coastal Research*, pp: 1619–1623.

Vesanto, J., Himberg, J., Alhoniemi, E., and Parhankangas, J. (2000). *SOM Toolbox for Matlab 5.* Relatório técnico, Helsinki University of Technology, 59 p.

Vis, G. J., Kasse, C., Kroon, D., Jung, S., Zuur, H., and Prick, A. (2010). Late Holocene sedimentary changes in floodplain and shelf environments of the Tagus River (Portugal). *Proceedings of the Geologists' Association*, 121(2):203–217, doi:10.1016/j.pgeola.2009.12.003.

Warner, J. C., Geyer, W. R., and Lerczak, J. A. (2005). Numerical modeling of an estuary: A comprehensive skill assessment. *Journal of Geophysical Research C: Oceans*, 110:1–13, doi:10.1029/2004JC002691.

Weaver, A. J. and Hsieh, W. W. (1987). Influence of Buoyancy Flux from Estuaries on Continental Shelf Circulation.1987. Influence of Buoyancy Flux from Estuaries on Continental Shelf Circulation. *Journal of Physical Oceanography*, 17(11):2127–2140, doi:dx.doi.org/10.1175/1520-0485(1987)017<2127:TIOBFF>2.0.CO;2.

Willmott, C. J. (1981). On the validation of models. *Physical Geography*, 2:184–194, doi:10.1080/02723646.1981.10642213.

Yankovsky, A. E. (2000). The cyclonic turning and propagation of buoyant coastal discharge along the shelf. *Journal of Marine Research*, 58:585–607, doi:10.1357/002224000321511034.

Yankovsky, A. E. and Chapman, D. C. (1997). A Simple Theory for the Fate of Buoyant Coastal Discharges. *Journal of Physical Oceanography*, 27(7):1386–1401, doi:10.1175/1520-0485(1997)027<1386:ASTFTF>2.0.CO;2.